SHELL-SIDE CHARACTERISTICS IN

A LEAK-PROOF HEAT EXCHANGER

BY

B. SHORT.

A thesis submitted to the Faculty of Graduate Studies and Research in partial fulfilment of the requirements for the degree of Master of Engineering.

Department of Mechanical Engineering,
McGill University,
Montreal.

April 1961

Table of Contents

List of Illustrations

Acknowledgements.

The author wishes to express his gratitude to Professor J.W. Stachiewicz for the advice and assistance received in the performance and presentation of this work. Mr. J. Kelly's aid, in the manufacture of the heat transfer probe, is appreciated. Thanks are also due to Miss J. Archer for typing this thesis.

The financial assistance of the National Research Council of Canada is gratefully acknowledged.

Nomenclature

A_c - crossflow zone flow area - $ft.^2$

A_f - flow sub-zone flow area - $ft.^2$

A_m - geometric mean flow area, $(A_c, A_w)^{0.5}$ - $ft.^2$

A_w - window flow area - $ft.^2$

a - exponent of Re in heat transfer equation

a_c - effective heating area of probe - $ft.^2$

a_f - effective flow area past probe - $ft.^2$

b - exponent of P_r in heat transfer equation

C, C_1, C_2 - constants in heat transfer equation

c - specific heat at constant pressure - BTU/°F - lb.

D - Depth of diameter or shell - ft.

d - outside or diameter of tube or coil - ft.

d_e - equivalent diameter, 4xflow area ÷ wetted perimeter - ft.

E_1 - Potential drop across current shunt - volt

E_4 - potential drop across centre section of probe - volt

f( ) - mathematical function

G - mass velocity - lbs./$ft.^2$, hr.

G_c - crossflow mass velocity based on A_c - lbs./$ft.^2$, hr.

G_f - flow sub-zone mass velocity based on A_f - lbs./$ft.^2$, hr.

G_m - geometric-mean mass velocity based on A_m - lbs./$ft.^2$, hr.

G_w - window mass velocity based on A_w - lbs./$ft.^2$, hr.

h	-	local heat transfer coefficient	-	BTU./hr.,^{o}F, ft.^{2}
h_c	-	average heat transfer coefficient in crossflow zone	-	BTU./hr.,^{o}F, ft.^{2}
h_o	-	overall average heat transfer coefficient	-	BTU./hr.,^{o}F, ft.^{2}
h_w	-	average heat transfer coefficient in window zone	-	BTU./hr.,^{o}F, ft.^{2}
$\bar{h}_m$	-	local measured heat transfer coefficient	-	BTU./hr.,^{o}F, ft.^{2}
I	-	current through coil	-	ampere
k	-	thermal conductivity	-	BTU./hr.,^{o}F, ft.
L	-	Baffle spacing	-	ft.
l	-	probe length	-	ft.
M	-	voltage multiplier constant	-	
n	-	exponent of A_r in modified heat transfer equation		
Q	-	heat transfer rate	-	BTU's/hr.
R	-	resistance of coil	-	ohm
R_s	-	resistance of current shunt	-	ohm
S_t	-	total heat transfer area in baffle section	-	ft.^{2}
S_w	-	total window zone heat transfer area	-	ft.^{2}
t_a	-	temperature of air	-	^{o}F.
t_c	-	temperature of coil	-	^{o}F.
Δt	-	temperature rise in air passing over coil	-	^{o}F.
α	-	thermal resistivity of coil	-	ohms,/^{o}F.
θ	-	temperature difference between coil and air	-	^{o}F.
μ	-	viscosity of shell-side fluid at bulk temperature	-	lbs./ft., hr.

μ_w - viscosity of shell-side fluid at tube wall temperature - lbs./ft., hr.

Dimensionless Numbers and Ratios

A_r - area ratio - $\frac{A_c}{A_w}$

L/D - spacing ratio

J_h - heat transfer factor $\frac{Nu}{Pr^{\frac{1}{3}} (\frac{\mu}{\mu_w})^{0.14}}$

J'_h - modified heat transfer factor $(\frac{J_h}{A_r^{\,n}})A_r^{0.126}$

Nu - Nusselt Number $\frac{h\,d}{k}$

P_r - Prandtl Number $\frac{c\,\mu}{k}$

Re - Reynolds' Number $\frac{G\,d}{\mu}$

Subscripts

c crossflow zone average

f flow sub-zone average

m geometric-mean average

w window zone average

Abstract

A model, two-dimensional leak-proof, heat exchanger was built. Local shell-side, heat transfer coefficients were measured in a typical section between two segmental baffles. Three baffle spacings, with five flow rates at each spacing, were used.

The results indicate that the crossflow region can be divided into a dead zone and flow zone. The size of these sub-zones is a function of the area ratio, A_r, and thus the average coefficient is also a function of A_r.

A single correlation, to express the average coefficient at various baffle spacings, was obtained by deriving a modified heat transfer factor, J_h'. Heat transfer rates can be correlated by $J'_{h_c} = 0.868\ Re_c^{0.490}$ for the crossflow zone, while window zone coefficients can be expressed by $J'_{h_w} = 0.721\ Re_m^{0.490}$, to within $\pm$ 5 per cent. This verifies experimentally that, while Re_c is the correct parameter for the crossflow zone correlation, Re_m should be used for the window zone.

INTRODUCTION

To determine the overall performance of a cross-baffle, shell-and-tube heat exchanger, the designer must be able to estimate the convective heat transfer coefficients on the tube and shell sides. Fluid flow inside a cylindrical tube has been thoroughly investigated, and good agreement exists between theoretical analysis and experimental results. Figure 1 illustrates that tube-side flow is divided equally among the tubes, making a single pass, and is similar to flow in a single tube. Thus tube-side calculations are comparatively simple.

Shell-side flow, shown in figure 2, is more complex. The fluid enters the first baffle section and flows normal to the tube bundle till it reaches the window of the first baffle. It then passes through a series of typical baffle spacings to the last baffle window and exits at right angles to the tube bundle, through the last section. The initial and final zones usually need separate consideration, due to entry and exit conditions requiring non-typical baffle spacing.

In a typical baffle section, (figure 3), the main body of the fluid enters through a window, at some stage is parallel to the tubes, turns, flows across the tube-bundle

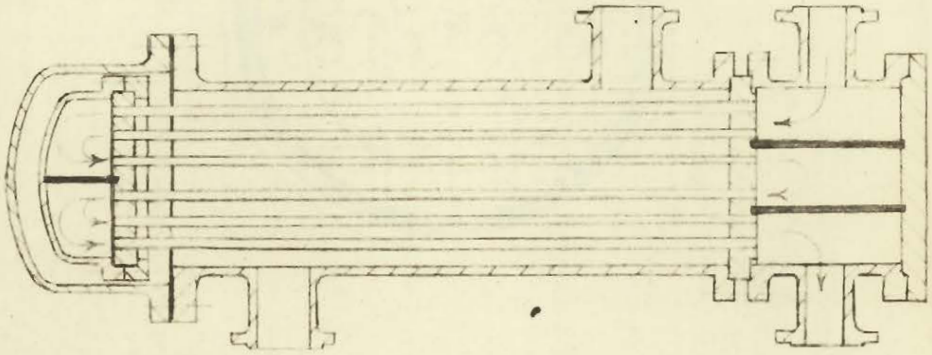

Figure 1.

Tube-side Flow

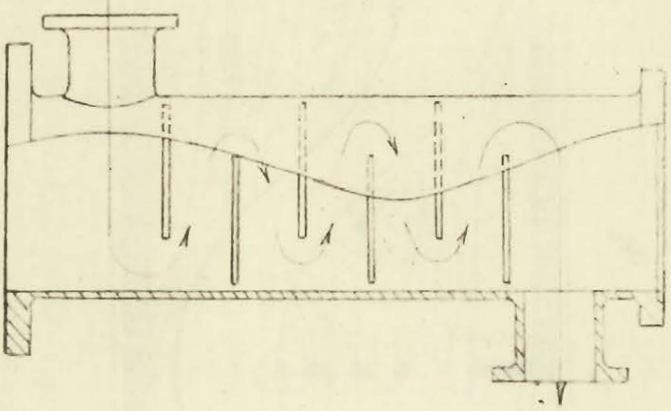

Figure 2.

Shell-side Flow

and turns to leave the section at the next baffle window. Since most shells are cylindrical, flow across the tubes is complicated by being three-dimensional. Also the tube-bundle pattern cannot be completed to the baffle boundary, thus allowing a portion of the fluid to by-pass the tube bundle. Further leakages occur in the clearance spaces between the baffle and the shell and between the tubes and the baffle tube holes.

Correlations, based on experiments carried out with one-dimensional flow parallel, normal, and at various angles to rectangular tube-banks, exist. By considering the main flow to be portions of these ideal conditions, experimenters have used various approximate methods to obtain shell-side correlations. Additional information for conditions between the ideal cases and actual heat exchangers may permit improvement in these methods. Therefore, the purpose of this work is to determine the effect of baffle spacings on local shell-side characteristics in a two-dimensional leak-proof heat exchanger between two typical baffles.

Description of Apparatus

Heat Exchanger

A model leak-proof heat exchanger of rectangular cross-section (Fig. 4), was built to provide a comparable test section. It consisted of a tube-bundle supported by four baffles with a tube-plate at one end, and a rigid top and bottom with two removable side plates.

The tube bundle consisted of 1/2 inch diameter tubes, spaced on 3/4 inch triangular pitch eighteen rows deep, with eight tubes per row. On the left-hand side of the first, ninth, eleventh and seventeenth rows, and on the right-hand side of the second, eighth, tenth and eighteenth rows, the outside tube was replaced by a 5/16 inch diameter steel rod threaded at both ends. Three groups of 1/2 inch diameter spacer tubes, to fit over the steel rods between the baffles, were machined to within 0.002 inches of the necessary length to give the desired baffle spacings. With the tube-bundle, tube-plate and baffles in position the spacer tubes were locked in position by tightening a nut on both ends of the steel rods.

Each baffle consisted of a 1/16 inch thick silicone rubber gasket sandwiched between two steel plates of the same thickness, while the tube-plate was made up of a 1/32

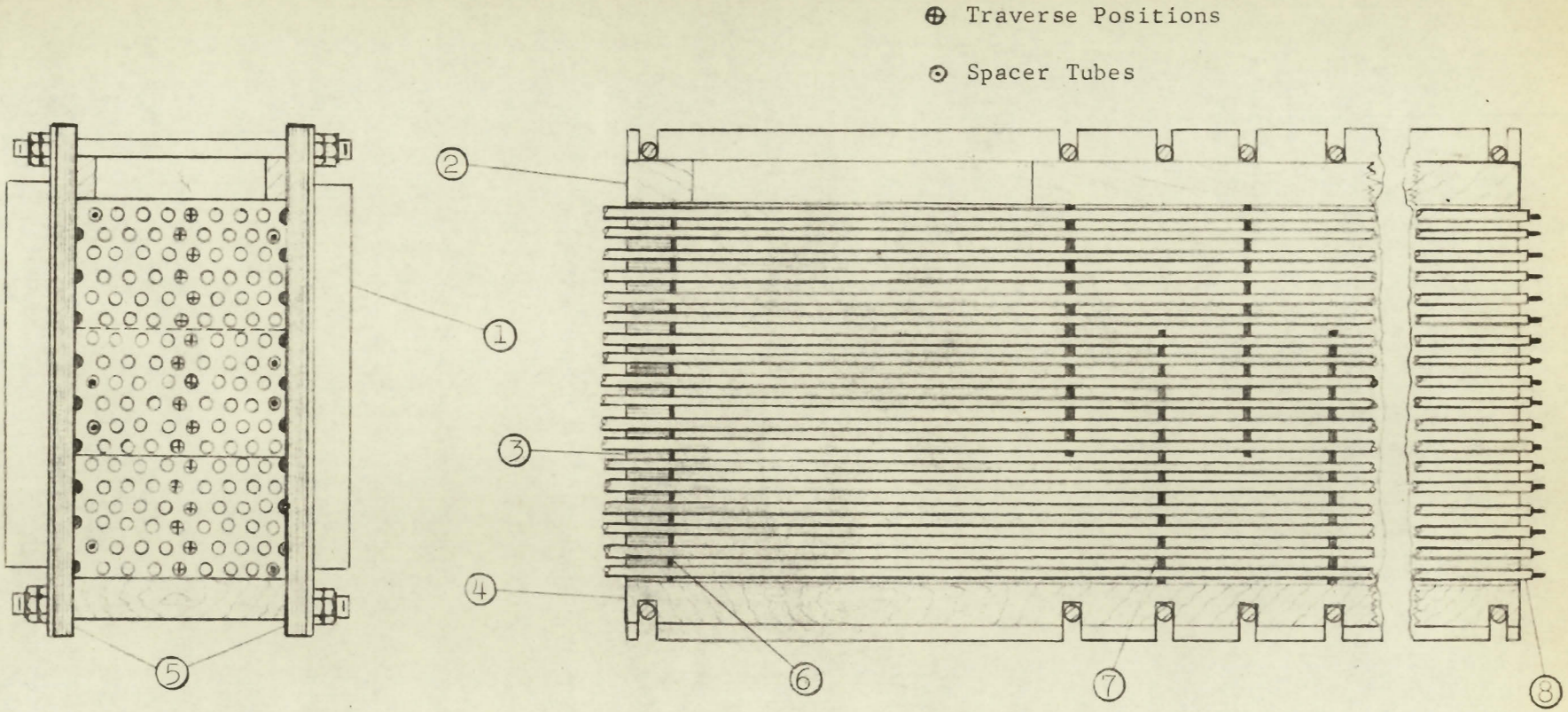

LEGEND

1. Side-Plate Clamps
2. Shell Top
3. Wooden Tube Plate
4. Shell Bottom
5. Shell Side Plate
6. Steel Tube Plate
7. Leak Proof Baffle
8. Tubes

FIGURE 4: CROSS-SECTION OF APPARATUS

inch rubber gasket between a 1/16 inch steel plate and a 1 inch thick piece of wood. The tube holes in the steel plate and wood block were all drilled at the same time in a special drill jig. The holes in the steel plate were then reamed to 33/64 inch diameter. Each row in the steel plates had an additional half-round hole so that the baffles could fit over half-rounds located on the side plates. The silicone rubber gaskets were cut to extend 1/16 inch over those edges of the baffle plates which touched the shell wall, while the tube-plate gasket was cut to fit the wood block. The gaskets were then cemented to one of the plates making up each of the baffles and the wood block. Using the holes in the wood block and the steel plates to locate special punches, 15/32 inch diameter holes were punched in the gaskets at each tube location and 9/32 inch diameter holes at each steel rod location. The other steel plate was then cemented to each gasket.

The shell-top and bottom were made of 1 inch maple while the side plates were made of 1/2 inch plywood. The top and bottom were attached to the wood tube-plate by glue and wood screws and the assembly was bolted to a stand. A rectangular hole 10 by 5 1/2 inches was cut in the top to provide an entrance for the air flow. On the side plates, half-round 1/2 inch diameter wood moulding was glued to

complete the tube pattern of each row of tubes. The sides were held in position by special clamps. All internal wood surfaces were sanded, given a coat of shellac, and waxed to provide a smooth surface.

Air Supply

Air was supplied to the shell side of the exchanger by a 1.1 p.s.i., 1500 c.f.m. centrifugal blower driven by a 10 H.P. electric motor. The exchanger was connected to the pressure side of the blower by 8 inch diameter steel piping, which had a straight section, 14 feet long. In the centre of this straight section, provision was made for the installation of sharp-edged orifices, in accordance with British Standard 1042 for D and $\frac{D}{2}$ taps.(1).Four plates with 1 5/8, 2 3/4, 3 1/4 and 4 1/2 inch orifices were used. The orifice taps were connected to manometers mounted on a vertical board, so as to measure the upstream static pressure before the orifice, and the differential head across the orifice, in inches of water.

A butterfly valve, driven by a Minneapolis Honeywell Modutrol control motor, was installed on the suction side of the blower, in order to obtain, and maintain, the various desired flow rates. The air temperature, at the outlet end of the exchanger, was measured by a mercury thermometer marked in 0.1 ^{o}C gradations.

Heating Coils

Local shell-side heat transfer coefficients were obtained by replacing a tube in the test section of the heat exchanger, with a closely wound fine wire electric coil of the same outside diameter as that of the tubes, and measuring its power dissipation and surface temperature. Figure 5 shows a cross-section through the probe. The outside diameter of the coil core (a phenolic-bonded paper based fibre) was reduced in the coil region, so that a coil (A) wound of No. 30 gauge enamel-coated copper wire, would extend beyond the surface of the core by 0.002 inches. Four 1/32-inch holes were drilled in the core to permit access to the coil's voltage (B) and current (C) taps, through the core's hollow centre. The core's diameter, at the ends, was turned down on a lathe, to give a press-fit with the inside of the tube-bundle tubes (D).

Two sets of coils were wound, one for the 20 per cent and 60 per cent baffle spacing tests, and the other for the 100 per cent baffle spacing tests. The former consisted of a centre section approximately 0.270 inches long, with guard rings of approximately the same length at either end, while the latter had a centre section approximately 0.530 inches long, with guard rings the same length as the former.

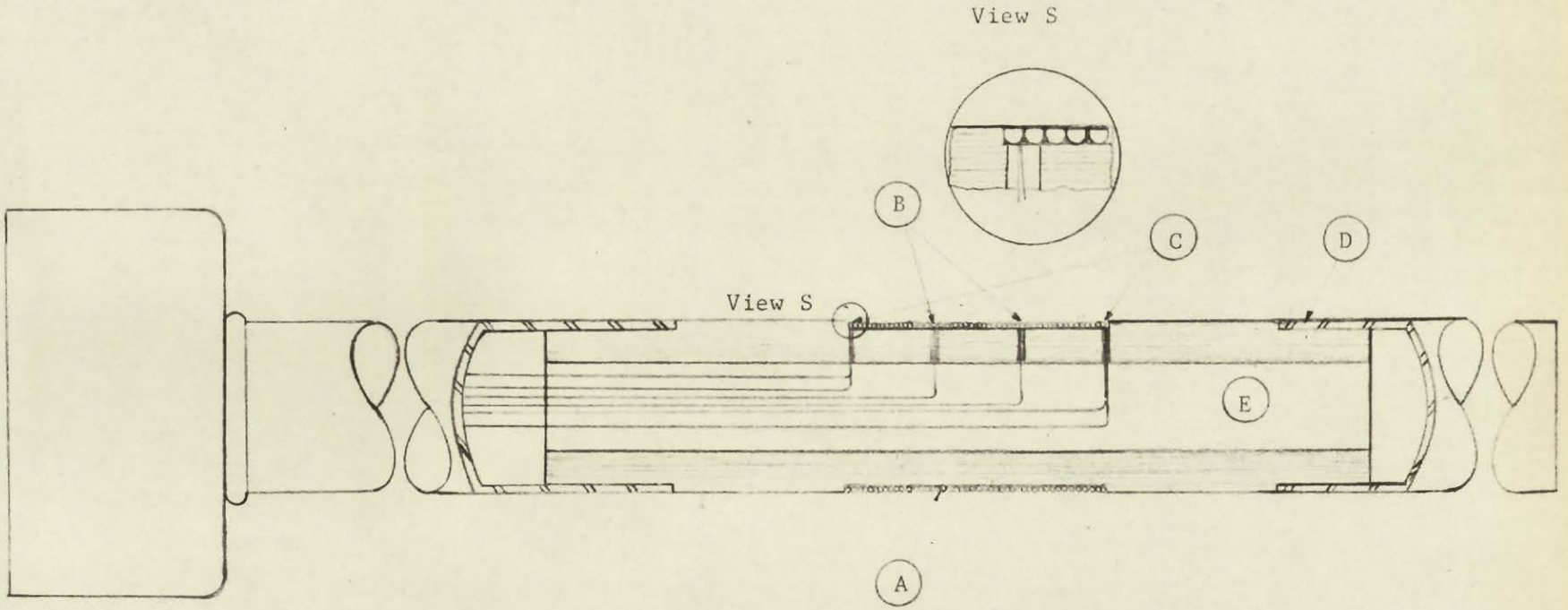

FIGURE 5: HEAT TRANSFER PROBE

Current leads, of No. 16 gauge insulated copper wire, were brought from the coil ends, into the hollow core centre,(E) and thence to the end of the core. Voltage taps, of No. 30 wire, were taken from the coil through all four holes. The current and voltage wires were then passed through the inside of a 48 inch long, 1/2 inch diameter tube, and connected to a nine-contact plug. The steel tube was then press-fitted to the coil core. Another 1/2-inch diameter steel tube 20 inches long was fitted to the other end of the core.

The coil was then given a heavy coat of shellac. After the shellac had hardened, the coil diameter was reduced to the tube diameter with emery paper. This was done to increase the copper surface exposure to the outside, and to simulate the surface of a smooth 1/2-inch diameter tube. The diameter of the coil was then measured with a micrometer, and the lengths of the various coil sections were determined with a sight gauge held on a lathe's micrometer feed.

The electrical circuit, shown in figure 6, was employed in order that the current through the coil, and the voltage drop across either end section, the centre section, or the whole coil, could be determined. A Brown Electronik precision potentiometer, with a scale of 0 - 20 millivolts, and an accuracy of 0.02 M.V., was used to determine voltage

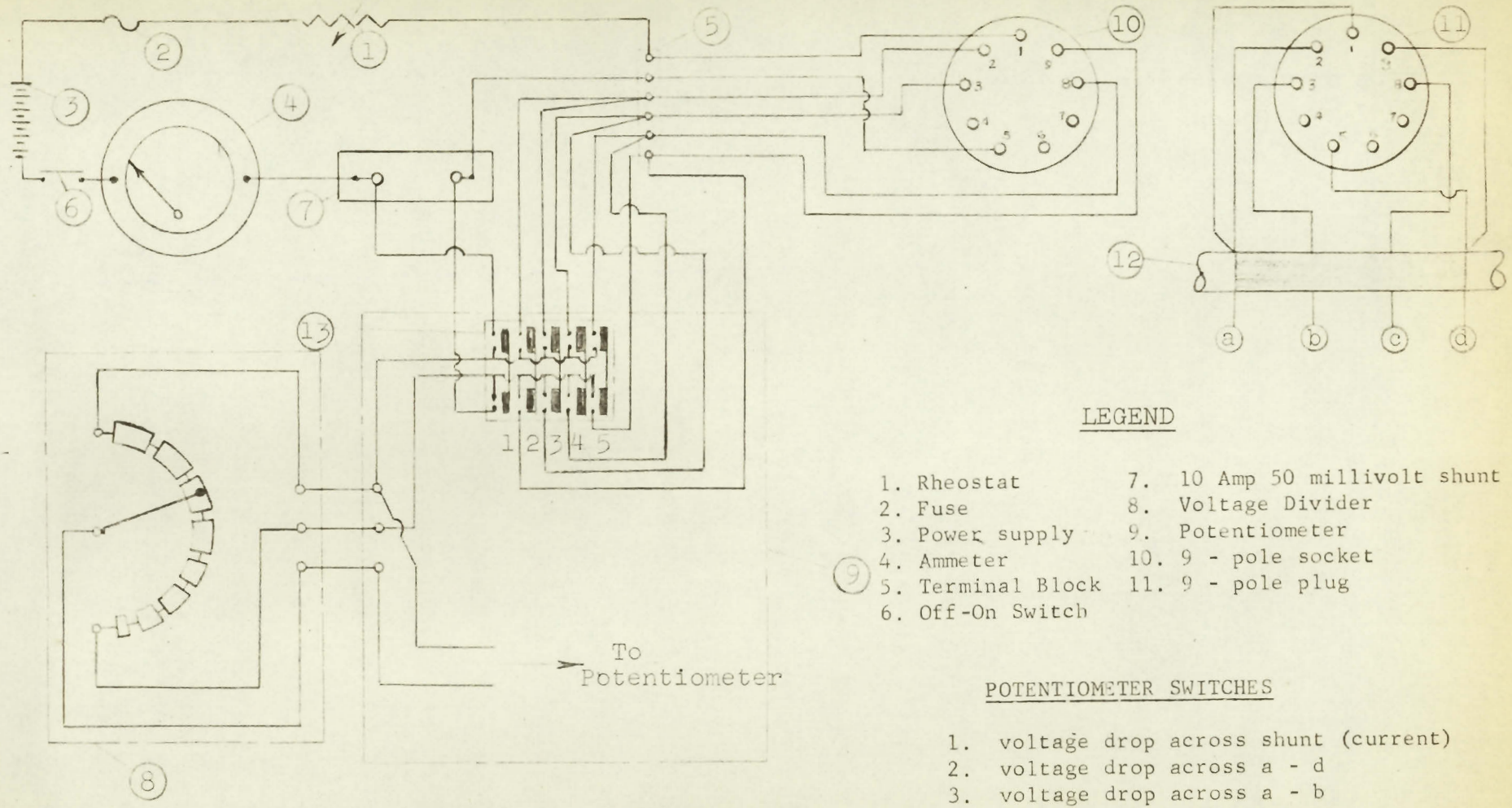

LEGEND

1. Rheostat
2. Fuse
3. Power supply
4. Ammeter
5. Terminal Block
6. Off-On Switch
7. 10 Amp 50 millivolt shunt
8. Voltage Divider
9. Potentiometer
10. 9 - pole socket
11. 9 - pole plug

POTENTIOMETER SWITCHES

1. voltage drop across shunt (current)
2. voltage drop across a - d
3. voltage drop across a - b
4. voltage drop across b - c
5. voltage drop across c - d

FIGURE 6: MEASURING CIRCUIT

drops across the various sections of the coil, and across the current shunt. The shunt was calibrated and found to have a potential drop of 5.12 M.V. per amp., to an accuracy of 0.2 per cent. The Fisher Ayton shunt was connected to the potentiometer so as to act as a voltage divider. A 0-10 ohm rheostat was used to set desired current readings, approximately. Power was supplied by a Heathkit battery eliminator and filtered through a 6 volt battery.

From the voltage and current readings, the resistance and power dissipation of any coil segment could be determined. Since the resistance of the coil is a linear function of its temperature, the average temperature of any coil segment could be calculated.

Test Procedure

(a) Coil Calibration

In order to use the heating coils as resistance thermometers, the resistance of each one had to be calibrated over the temperature range to be used in the heat transfer tests. The current shunt shown in the wiring diagram, figure 6, was replaced by one having a resistance of 2.003 ohms and a 650 ohm resistance was placed in series with the current supply. The Ayrton shunt was removed from the circuit as the voltage drop across the new shunt and coil segments was within the range of the potentiometer.

The coil was submerged in an oil bath which rested on an electric hot plate. Current was supplied to the hot plate from a 0 - 130 volt variable transformer, so that the heating rate to the oil bath could be adjusted to equal its heat dissipation to the surroundings at various temperatures. The hot plate current was then turned on and the oil was continually agitated. The bath temperature was measured by a standardized mercury thermometer. When the oil bath reached and maintained a constant temperature for a period of five minutes, current of about 0.008 amperes was supplied to the coil. A set of readings was taken, giving the voltage drop across each coil segment, the whole coil, and the current shunt. The coil current was then shut off and the variable transformer was set at a new value to give a

higher temperature. This procedure was continued, in approximately 15°C. temperature steps, until a temperature of 95°C. was reached. The coil was then removed from the bath and cleaned.

The values of coil resistance were then plotted against temperature and found to give a straight line relationship, accurate to within $\pm$ 0.5°C. for the centre section of the coil. The coefficient of temperature resistivity, for the various coils tested, varied from 0.00385 to 0.00396 ohms per ohm per °C. from 20°C. This compares favourably with the handbook value of 0.00393 ohms per ohm per °C. for pure copper.

(b) Operating Procedure

The test section consisted of the space between the second and third baffles of the heat exchanger. When the exchange was being assembled for a desired baffle spacing, the coil-and-tube assembly was inserted in place of the centre tube of the seventh row. The coil was positioned so that the starting edge of its centre section was aligned to the second baffle, with the rest of the segment extending into the test section. A mark was then scribed on the steel tube portion of the assembly where it was aligned with the

outside surface of the tube-plate. The coil-and-tube assembly was then removed from the exchanger and a scale of traverse positions was marked on the steel tube, using the micrometer feed of a lathe. Traverse positions for the 20 per cent and 60 per cent spacings were 0.260 inches apart, while the 100 per cent ones were 0.520 inches apart.

After the exchanger was completely assembled, and the desired orifice plate was in place, the fan was turned on and the butterfly-valve motor control switch was adjusted until the orifice differential pressure, for the required mass velocity, was obtained. Since only a small portion of the fan capacity was being used, "choking" of the air supply resulted in heating up the air to about 10°C. above ambient temperature. Therefore a warming-up period of one hour was required before the air temperature became reasonably steady.

The coil-and-tube assembly was then inserted in the centre tube position of the first row and adjusted so that the scribed mark for the first traverse position was against the tube-plate. The current was then turned on and adjusted to give a temperature between 70°C. - 100°C. on the coil surface. After the current had been on 5 minutes, voltage and current readings were taken with the Ayrton shunt set so that the voltage drop readings were in the 10 M.V. to 20 M.V.

portion of the potentiometer range. Readings were then taken at one minute intervals until they became steady. The outlet air temperature was noted and the coil was then moved to the second traverse position, with the current still on. Readings were again taken at one minute intervals until constant conditions were obtained, and the outlet air temperature was again recorded. Readings for each position of the first row tube were taken in this manner. The current was then shut off, the coil-and-tube assembly removed from the exchanger, and the steel tube was replaced in the position vacated. The coil-and-tube assembly then replaced the steel tube in the centre of the second row, the current was turned on, and the traverse was taken in a manner similar to that used in the first row.

Centre tube positions of each window row were likewise traversed. Additional spot readings were taken upstream and downstream of the test section. In the cross-flow area traversing was done in the same manner, until positions of near constant heat transfer were reached. Then every fourth traverse position was checked. The orifice static and differential manometer readings were recorded before and after each row was traversed, and the barometric pressure was checked after every three rows. In this manner local heat transfer readings were taken at five

velocities for each baffle spacing. Approximately 5000 local heat transfer coefficients were obtained.

(c) Accuracy of Results

Local average heat transfer coefficients were determined from

$$\bar{h}_m = \frac{3.413\ E_1\ E_4\ M}{1.8\ R_s\ \pi\ dl\ (t_c - t_a)}$$

The voltage drops across the current shunt (E_1) and the centre section of the coil (E_4) were read to an accuracy of 0.02 millivolts in 10 millivolts. The voltage multiplier constant (M) and the current shunt resistance (R_s) were calibrated to within 0.5 per cent and 0.2 per cent of their values respectively. The overall precision of the heat dissipation was therefore estimated as being within 1.1 per cent.

The coil diameter (d), and the centre section length (l), were measured to within 0.0005 and 0.002 inches, in 0.500 and 0.300 inches, respectively. The heat dissipation area was therefore determined to an accuracy within 0.8 per cent.

The temperature of the coil (t_c) could be determined to an accuracy of 1° C. and that of the air (t_a), 0.1° C. The minimum temperature difference between the coil and air was found to be 30° C. and the discrepancy of temperature affected the value of local heat transfer ($\bar{h}_m$) by 3.7 per

cent. The total accuracy of heat transfer measurements is therefore estimated as being within $\pm$ 5.6 per cent.

Two further discrepancies appear possible in determining heat transfer coefficients in this manner. Firstly, the air passing over the coil will be heated and the thermal energy, thus gained, will not be dissipated immediately. Thus air surrounding the coil will be at a temperature higher than that measured by the thermometer

$$Q = c\ G\ a_f\ \Delta t$$

$$= h\ a_c\ \theta$$

$$\text{therefore } \frac{\Delta t}{\theta} = \frac{h\ a_c}{c\ G\ a_f}$$

$$\text{for our case } = \frac{2\ \pi\ h}{c\ G}$$

but h is proportional to G^a where a is less than one. If the same quantity of heat is transferred at different mass velocities

$$\frac{\Delta t}{\theta} = \frac{a_c}{c\ a_f\ G^{(1-a)}} \text{ X constant}$$

Therefore, the relative error in measuring temperature difference tends to occur at lower mass velocities. For the minimum mass velocity of 6,000 pounds per square foot-hour, and average heat transfer coefficient of 21.5 B.T.U'S per square foot-hour-^oF. at this velocity

$$\frac{\Delta t}{\theta} = \frac{2\ \pi\ x\ 21.5}{0.24\ x\ 6000}$$

$$= 0.095$$

However, this relative rise takes place after the air has completely passed the coil. The error in temperature difference would then be + 4.75 per cent, causing the measured heat transfer coefficient to be the same percentage lower.

A second error that might occur is the presumption that the average coefficient for the coil is based on a constant coil temperature. The measured coefficient for a unit length coil is

$$\bar{h}_m = \frac{I^2 R \times 3.413}{\pi D \bar{\theta}}$$

If $\bar{h}_m$ = measured heat transfer coefficient B.T.U.'s per $^oF.$ - radian-wire diameter

r = resistance of wire, ohms per radian

θ = local temperature difference between coil and air, $^oF.$

x = angular length of coil, radians

Then for one wire

$$\bar{h}_m = 3.413 \frac{\int_o^\pi I^2 r \, dx}{\int_o^\pi \theta \, dx} = \frac{3.413 \, I^2 r}{\bar{\theta}}$$

where $\bar{\theta}$ is the average temperature difference between coil and air.

However the average coefficient $\bar{h}$ is

$$\bar{h} = \frac{\int_o^\pi h \, dx}{\pi}$$

where h is the local heat transfer coefficient

$$\bar{h} = \frac{3.413}{\pi} \int_o^\pi \frac{I^2 r}{\theta} \, dx$$

Assuming constant resistance

$$\bar{h} = 3.413 \frac{I^2 r}{\pi} \int_0^{\pi} \frac{dx}{\theta}$$

If θ is constant

$$\bar{h}_m = \bar{h}$$

Consider a small wire portion of angular length dx with a conductance equal to k B.T.U.'s - radians per ^{o}F.

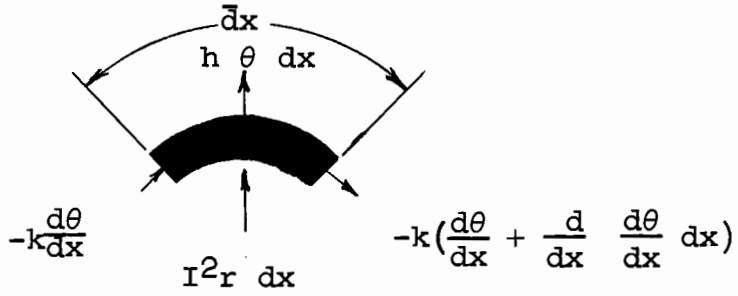

Then $3.413\ I^2\ r\ dx + k\ \frac{d^2\theta}{dx^2}\ dx = h\theta\ dx$

Where h and θ functions of x.

but $\bar{h}\ \bar{\theta} = 3.413\ I^2\ r$

then $\frac{d^2\theta}{dx^2} + a = b\ h\ \theta$

where $\frac{\bar{h}\ \bar{\theta}}{k} = a$ and $\frac{1}{k} = b$

Measurements of heat transfer coefficients around a tube show that the minimum may vary as much as 40 per cent from the maximum. If the variation is assumed to follow a simple harmonic pattern, the local coefficient may be expressed as

$$h = \bar{h}\ (1 + \tfrac{3}{7} \cos.\ 2x)$$

This satisfies the boundary conditions that h is a maximum at the upstream and downstream stagnation points, and is a

minimum midway between. It may be assumed that the temperature follows a similar law. However, maximum temperature should occur at the place where minimum heat transfer is located.

As a first approximation let

$$\theta = \bar{\theta} \ (1 - c \cos 2x)$$

where "c" is some constant to be determined. If the substitution for a, h, θ, $\frac{d^2\theta}{dx^2}$ are made in the above differential equation

$$c = \frac{\frac{3}{7} b \bar{h}}{4 + b \bar{h} + \frac{3}{7} b \bar{h} \cos 2x}$$

At first sight it would appear that c is a variable. However before making a second approximation, values for b and $\bar{h}$ are substituted to determine the variation in c

Maximum value $\bar{h}$ = 70 B.T.U.'s per ft.^{2}-hr.-$^\circ$F.

$$= \frac{0.01 \times 70}{144 \times 4} = \frac{1}{823} \text{ B.T.U.'s per radian -hr.-}^\circ\text{F}$$

For a coil made of 30 gauge copper wire wrapped around a 1/2 inch core K = 0.822 B.T.U.'s radians per $^\circ$F.-hr.

then c = 0.00015868 for cos 2 x = 1

and c = 0.00015871 for cos 2 x = 0

There is little value in attempting a second approximation and "c" may be assumed to be a constant equal to 0.00016.

$$\text{Therefore } \bar{h} = 3.413 \frac{I^2 r}{\pi} \int_0^{\pi} \frac{dx}{(1 - 0.00016 \cos 2x)\,\bar{\theta}}$$

$$\text{From integral tables } \bar{h} = \frac{I^2 r}{\pi \bar{\theta}} \frac{\pi}{(1 - 0.00016^2)}$$

$$= 1.00000001\ \bar{h}_m$$

Therefore the difference in value of measured coefficient from the actual coefficient is insignificant.

Since $r = \bar{r}\,(1 + \alpha\theta) = \bar{r}\,(1 + \alpha\bar{\theta} - 0.00016\,\alpha\bar{\theta}\cos 2x)$

and since $\alpha = 0.04$

the assumption of constant resistance around the circumference of the probe is reasonable.

Overall accuracy of heat transfer measurements is therefore + 5.6 per cent

- 10.4 per cent.

Theory

For sometime it has been known that the dynamic characteristics of a flowing fluid have a definite effect on the convective transfer of heat from a solid body to the fluid. Therefore, it is necessary to understand the general nature of fluid flow, in order to obtain a greater perception of the problem involved in studying shell-side properties in a heat exchanger.

In 1904 Ludwig Prandtl proposed the hypothesis "that for fluids of relatively small viscosity, the effect of internal friction is appreciable only in a narrow region surrounding the fluid boundaries". Provided the fluid boundaries are sufficiently far apart and the fluid density changes small, analysis of flow inside this "boundary layer" reveals the nature of resistance to heat transfer from a solid to a fluid.

In the region where the fluid first encounters the solid, the boundary layer is very thin and the flow is laminar. Downstream the boundary layer continues to grow until it eventually loses stability at a transition point, where the major portion of the flow becomes turbulent. Associated with the turbulent boundary layer is a very thin film next to the solid, termed the sub-layer, in which the flow is laminar.

Resistance to heat transfer is directly proportional to the boundary layer thickness for laminar flow. Since the growth rate of the turbulent boundary layer and its associate sub-layer, is considerably less than that of the laminar boundary layer, flow associated with the former has a greater heat transfer rate for fully developed flow. A similar argument shows that flow accompanied by a turbulent boundary layer has a greater pressure drop than that associated with a laminar boundary layer.

Analyses of flow over a flat plate are given by Eckert and Drake (2). These show, that at constant main stream velocity, the rates of pressure drop and heat transfer decrease as the square root of the downstream distance from the leading edge for laminar flow, while they diminish as the one-fifth power of the distance for turbulent flow.

If flow over a cylinder placed in a free stream is observed, an additional phenomenon is noted. At some point on the cylinder the boundary layer separates and a turbulent wake is formed on the downstream side. When the boundary layer is laminar the separation point tends to move upstream with increasing Reynolds number, due to decreasing momentum in the boundary layer. This continues until the transition stage is reached. In the turbulent boundary layer the loss of momentum is much less and the point of separation is farther downstream.

Figures 7A, 7B, and 7C show the wake formation for the three stages of flow.

Eckert (3) analyzed heat transfer for the laminar boundary layer formed at the surface of circular and elliptical cylinders in the region prior to separation. His results show that the heat transfer rate diminishes as the square-root of the distance from the stagnation point, measured along the surface of the cylinder. Unfortunately turbulent flow and the wake region have not been analyzed in a similar manner.

When the flow is too complicated to be analyzed mathematically a different approach is taken. In 1909 Nusselt made a dimensional analysis of the variables which might affect the heat transfer coefficient inside a pipe. He arrived at the expression

$$Nu = C\, R_e{}^{a}\, P_r{}^{b}$$

For fluids of high viscosity the correlating equation is modified so that

$$J_h = \frac{Nu}{P_r{}^{b}\ (\frac{\mu}{\mu_w})^{n}} = C\, R_e{}^{a}$$

Wherever the complicated nature of flow defies boundary layer analysis this is the usual form in which experimental results are expressed.

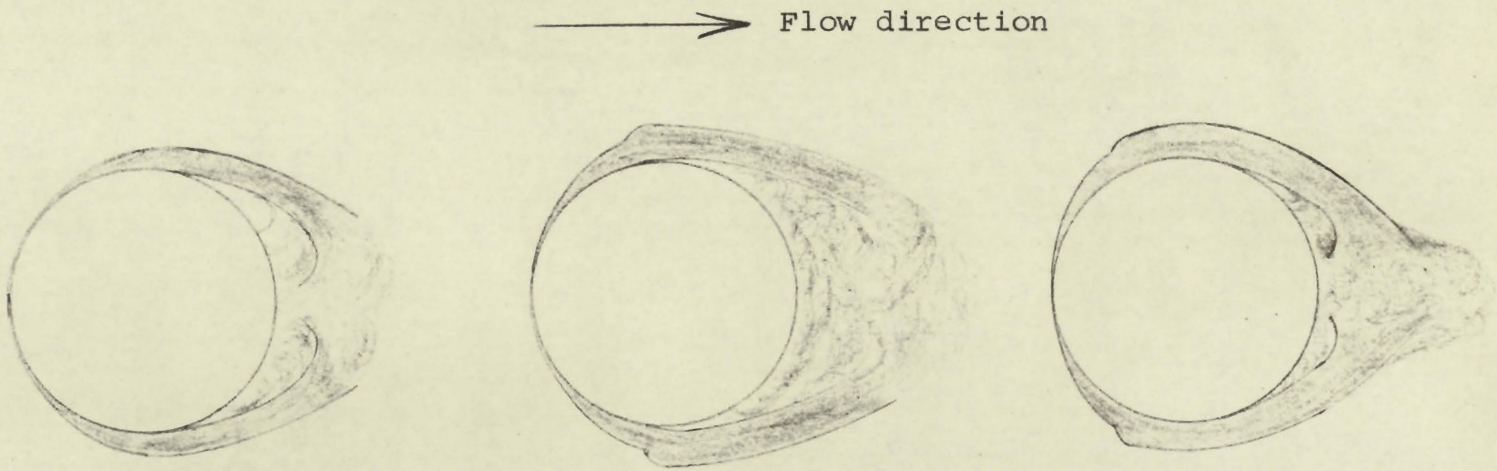

FIGURE 7: FLOW ACROSS CIRCULAR CYLINDERS

Figure 8 shows the local heat transfer variation around the circumference of a cylinder at Reynolds numbers corresponding to those in figure 7. Since the flow at the first and second Reynolds'numbers is laminar to the separation point, the heat transfer decreases in accordance with Eckert's analysis. Also the separation point, at the higher of the two numbers, is farther up stream, resulting in minimum heat transfer occurring earlier. The flow at the highest Reynolds' number becomes turbulent before separation, and minimum heat transfer occurs at the transition point. At this point there is a sudden rise in heat transfer in a manner similar to that of the flat plate. Heat transfer then decreases to a second minimum at the separation point.

In the wake, heat is transferred by the rubbing action of the turbulent vortices which are formed on the rear side of the cylinder, and detach themselves to enter the main stream. At low Reynolds' numbers this action is slight and the heat transferred in the wake is much less than on the upstream side of the cylinder. However, the intensity of vortex motion is rapidly augmented with increasing Reynolds' number, with the result that heat transfer eventually equals and surpasses that on the upstream side.

Figure 9 is McAdams' (4) logarithmic plot of average

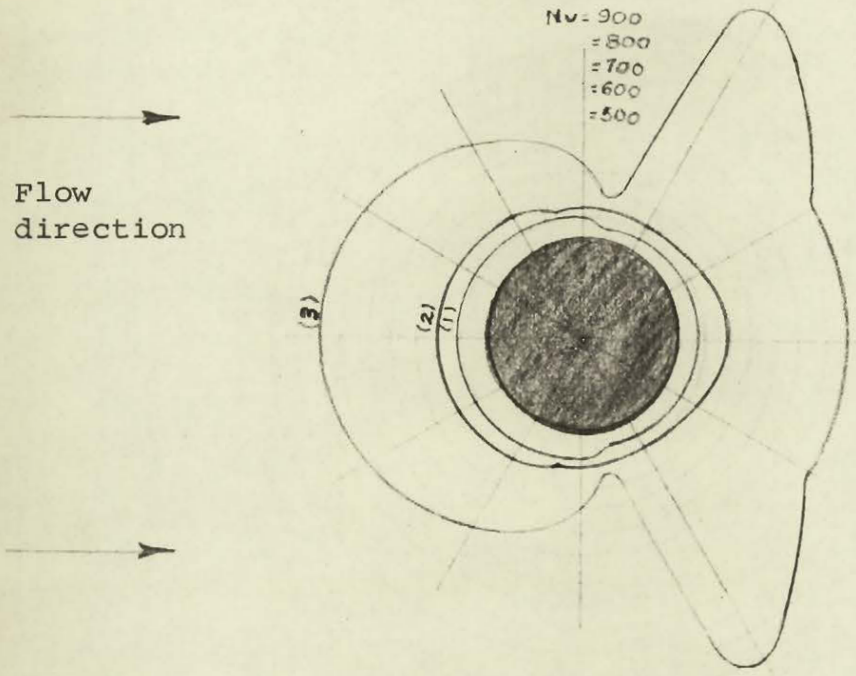

FIGURE 8: LOCAL HEAT TRANSFER AROUND CYLINDERS

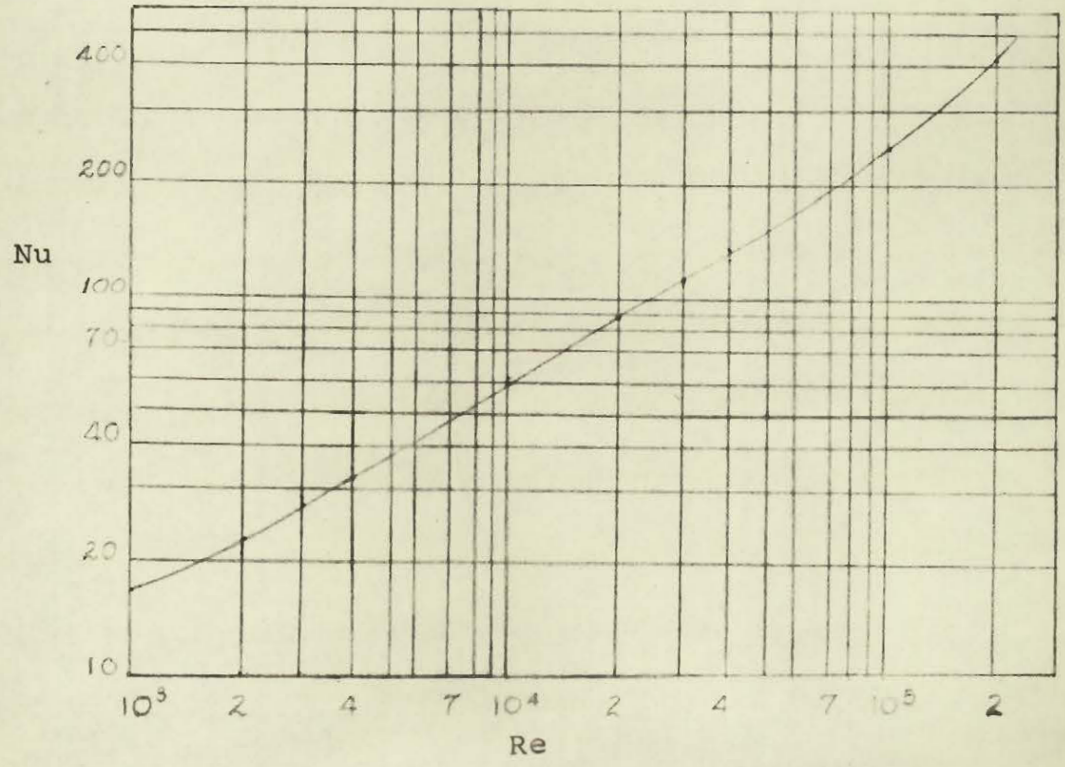

FIGURE 9: AVERAGE HEAT TRANSFER COEFFICIENTS FOR CYLINDERS.

heat transfer for flow over cylinders. These are the results of experiments carried out by several investigators over a range of Reynolds' number from 1,000 to 200,000. At the lower range the slope of the curve is 0.45, showing that the laminar boundary layer on the upstream side of the cylinder is the controlling heat transfer agent. At Reynolds' number equal to 200,000 the slope is 0.81, indicating the turbulent boundary layer and wake as being the principle heat transfer regions. Flow rates normally encountered in heat exchangers would be expected to produce laminar flow in the attached boundary layer.

When a flowing fluid enters an enclosed region the boundary layers generated at the walls grow and eventually meet. Downstream from this point, heat transfer and pressure drop rates remain constant. Provided transition has not occurred in the entrance length the flow will remain laminar, otherwise the fully developed flow is turbulent.

A negative pressure gradient occurs in the entry region due to boundary layers reducing the free stream area and thus increasing its velocity. This negative pressure gradient augments the boundary layer momentum and reduces its growth rate. Thus the decrease in heat transfer, downstream from entry, is greater for unbounded than enclosed flow. In the latter case, however, the negative pressure

gradient increases the overall pressure drop.

From experiments carried out with flow across tube banks it is found that heat transfer in the first rows is less than for the downstream rows while the pressure drop is much greater at entry than downstream. The former result is due to the main flow becoming turbulent shortly after entry. This turbulence is produced by the rough and twisting path which the fluid has to follow and the effect of the wake formed by the upstream tubes on those downstream. Due to the large negative pressure gradient at entry, pressure drops are greater prior to fully developed flow.

Figures 10A and 10B show the regions of the boundary layer and turbulent wakes for aligned and staggered tube spacing. From this it can be seen that the boundary layer and the wake region tend to fill the free stream area, somewhat more readily in the case of staggered spacing. It would therefore appear that the free stream velocity, and correspondingly the heat transfer and pressure drop rates, would be greater. Experimental results tend to support this supposition.

It appears that no rigid analysis has been made of flow past segmental baffles. However, in order to make a qualitative study of the flow patterns in typical baffle spacings, A.Y. Gunter et al(5) built a series of horizontal tubeless two-dimensional models. Fluid, with fine aluminum

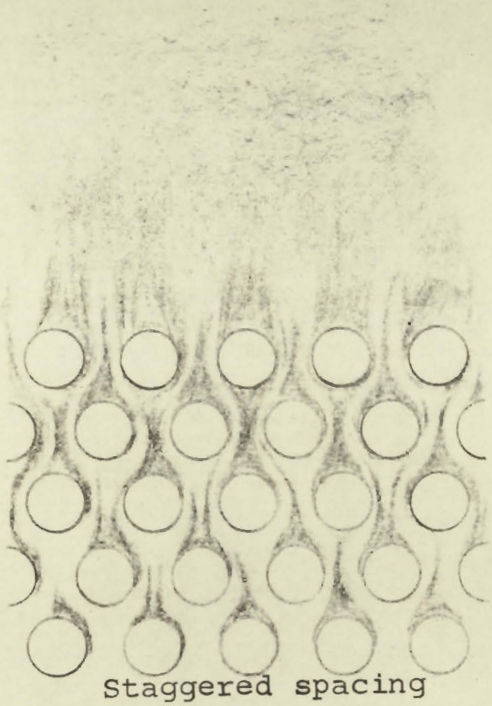

FIGURE 10A

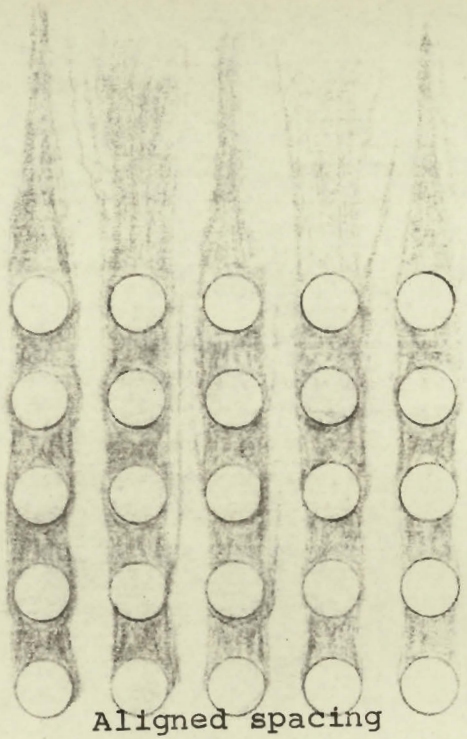

FIGURE 10B.

FIGURE 10: FLOW ACROSS TUBE-BANKS

powder suspended on the surface, was passed through the models. Photographs were taken to show the type of flow for various baffle spacings and window openings.

Figure 11 shows the flow for the three baffle spacings, with the single window opening, corresponding to those used in this experiment. The flow can be divided into two types: main stream flow and eddy flow, and the location, shape, and relative sizes vary for the different spacings.

In the crossflow zone the main stream fills only a portion of the area of the two larger spacings, while it completely fills the area of the smaller spacing, except for a small eddy near the entry baffle. In all cases there is a varying velocity across the main stream. The remainder of the cross flow region of the wider spacings is filled with eddy flow with the widest spacing having the biggest eddy.

In the exit window region of the widest spacing the eddy formed in the crossflow zone continues to the shell wall, while the main stream hugs the exit window baffle. In the same region of the middle spacing the main stream spreads to fill almost completely the window region. However near the corner formed by the up stream baffle and the shell the velocity is decreased and a small eddy is formed. In the entry window region of these two spacings, a small eddy is formed in the corner of the downstream baffle and the shell.

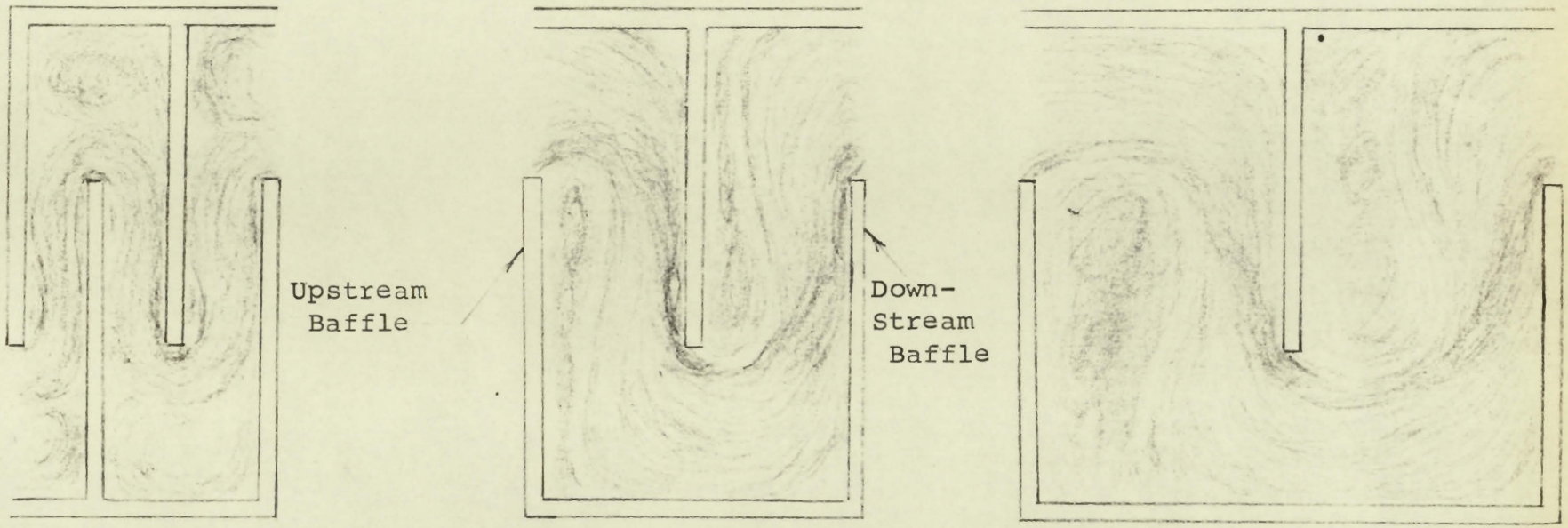

FIGURE 11: FLOW PAST TWO-DIMENSIONAL BAFFLES

Also a vena contracta is formed at the baffle cut and is much bigger for the largest spacing. In the window region of the smallest spacing the mainstream tends to hug the baffle. A large vortex is induced in the area closest to the shell with its centre above the baffle cut.

From this it could be assumed that those areas occupied by the mainstream would have characteristics similar to flow across tube banks. In the eddy regions it would be expected that the dependency on the flow rate would be reduced.

Also it can be seen that entry conditions to the crossflow and window zones are quite different from those occurring in one-dimensional studies of flow across banks of tubes. Heat transfer coefficients, in the initial rows of both zones, are most likely to be similar to those in the downstream rows, due to the turbulence created by the baffles and the changing direction of the fluid.

Review of Previous Work

Since the major portion of the shell-side fluid path is across the tube-bundle, heat transfer data, of flow across tubes, are of utmost importance. Many investigations have been made on flow at right angles to compact tube bundles, with various tube spacings and arrangements. In presenting their results the experimenters have varied the choice of velocity and characteristic length used in the construction of the Reynolds and Nusselt numbers.

In order to express this information in uniform terms, E.D. Grimison (6) correlated several researchers' results. As a reference velocity the average flow in the narrowest cross-section, between the tubes in the tube-bundle, was used, and for characteristic length the tube diameter, d. The ratios $\frac{S_1}{d}$ and $\frac{S_2}{d}$ describe the tube spacing. S_1 is the centre-to-centre distance between the tubes, perpendicular to the flow direction and S_2 is the centre-to-centre distance parallel to the flow direction. Figure 12 illustrates this for staggered and aligned tube pitch patterns. As interpolated from Grimison's values, at the tube pitch and Reynolds' numbers used in this experiment, the Nusselt equation for air is

$$Nu = 0.496\ R_e^{0.555}$$

The Reynolds' number exponents and Nusselt equation constants

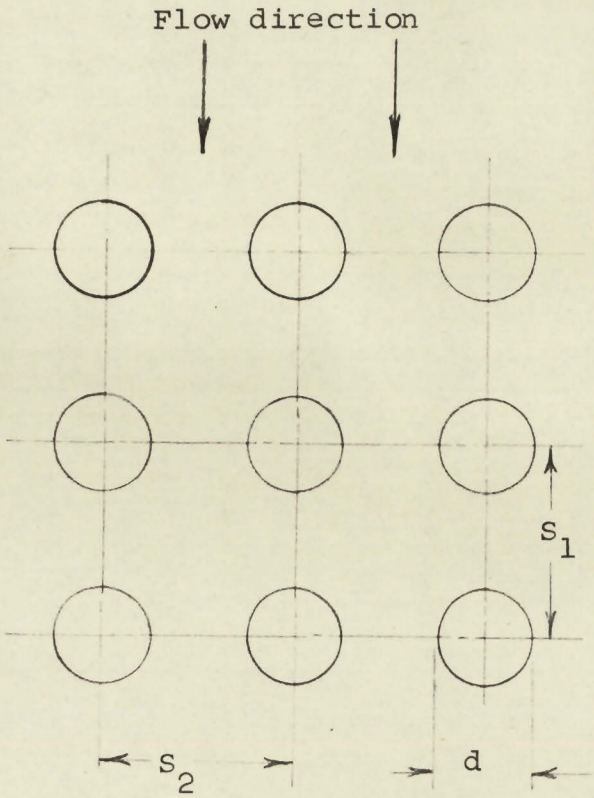

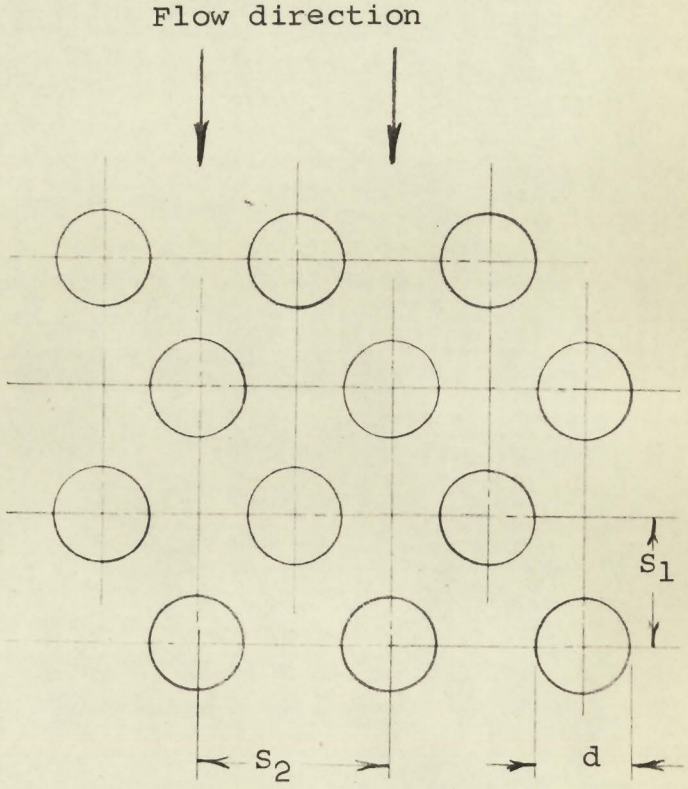

FIGURE 12: TUBE-BUNDLE ARRANGEMENT

for other pitches, usually found in heat exchangers, vary from 0.554 - 0.662 and 0.518 - 0.250 respectively.

G.A. Shaw (7) carried out a series of tests to find the effect of flow at angles, ranging from 20° to 90°, to a 10 row tube-bank. For a triangular tube pitch pattern, similar to the one used in this experiment, his heat transfer measurements for fully developed flow are represented within $\pm$ 10 per cent by

$$Nu = 0.451\ Re^{0.56}$$

The Reynolds' number is based on the cross-flow component of mass velocity across the narrowest cross-section of the tube-bank. In a similar manner he was able to correlate O.P. Ornatski's (8) results, based on angular flow heat transfer experiments, over a seven row, square pitch, tube-bank. For fully developed flow he obtained

$$Nu = 0.260\ Re^{0.624}$$

In order to obtain idealized conditions A.P. Bergelin et al. (9) built a cylindrical test heat exchanger, in which the baffle-tube holes, and baffle-shell clearance leakages were eliminated. An attempt was made to reduce the tube-bundle leakage by partially completing the tube pattern to the shell wall, with steel rods of somewhat smaller diameter than the tubes. Three different baffle spacings were tested, and three window sizes were used at each spacing. Overall heat transfer was measured in each case.

After accounting for the tube-side contribution to overall heat transfer, the average coefficient for the complete shell-side was obtained. In order to estimate heat transfer in the crossflow region it was assumed that heat transfer in the window region could be expressed by the crossflow correlation, provided the geometric-mean mass velocity was used in determining the window Reynolds' number.

Then $h_w = h_c \; A_r^{\frac{a}{2}}$

where a is the exponent of the Reynolds' number in the Nusselt equation. Also $h_o \; S_t = h_c \; S_t - h_c \; S_w + h_w \; S_w$

Therefore $$h_c = \frac{h_o}{1 - \frac{S_w}{S_t} + \frac{S_w}{S_t} A_r^{\frac{a}{2}}}$$

The values, thus obtained, bore fairly close agreement to Grimison's correlation for the Reynolds' number range above 5,000. However, the range is somewhat limited, reaching no more than 10,000. Also, only three results are given, in this range, for A_r greater than one, and two of the points fall below the correlating curve.

In an attempt to determine local shell-side heat transfer coefficients M.S. Gurashankariah and J.G. Knudsen (10) reported the results of tests carried out in a typical baffle spacing of a model heat exchanger. The cylindrical model consisted of fourteen tubes, with a baffle-tube hole clearance $\frac{1}{32}$ -inches, and a baffle-shell clearance $\frac{1}{16}$ inches.

Only two tubes were located in each window. The heat transfer readings were taken on all fourteen tubes at 3/4 - inch intervals for two baffle spacings and three velocities each. A sensing probe consisting of an electrical heating ribbon wrapped around a tube was used to determine heat transfer. Seven thermocouples, equally spaced around the circumference of the probe, determined the local temperature. Local coefficients were averaged for each probe location, and at each tube position.

The results indicate that the flow is divided into three zones: (1) the longitudinal zone in the baffle window, (2) the eddy-flow zone in the crossflow area nearest the upstream baffle, (3) the crossflow near the downstream baffle. Heat transfer coefficients in the eddy zone were somewhat higher than in the other two regions. The discrepancy between the crossflow and eddy zones tended to increase with baffle spacing and mass velocity. The longitudinal flow zone, relative to the overall average, tended to have higher coefficients at the wider spacing. Minimum heat transfer occurred in the centre of the baffle spacing of all crossflow tubes. In the window area the minimum point occurred 70 per cent downstream from the upstream baffle. The overall heat transfer was calculated and found to agree with

$$Nu = 0.21\ Re_m^{0.6}$$

Several people have attempted to correlate shell-side heat transfer rates based on tests carried out on operating heat exchangers. Of these, two deserve special mention.

Donohue (11), correlating the work of several experimenters, noted that when the baffle spacing was increased, coefficients of heat transfer, for the same cross-flow Reynolds' number, also increased. This suggested that increased window velocity augmented overall heat transfer. He therefore proposed the following correlation:

$$Nu = C\ Re_m^{0.6}\ Pr^{\frac{1}{3}}\ \left(\frac{\mu}{\mu_w}\right)^{0.14}$$

In determining the mass velocity characteristic he suggested that it be based on the geometric-mean of the window and crossflow zones. The geometric-mean area is obtained as follows:

$$(A_w \cdot A_c)^{0.5} = A_m$$

$$G_m = \frac{\text{mass flow}}{A_m}$$

All other terms in the Reynolds' number are the same as in Grimison's crossflow relations.

For narrow tube pitch Donohue suggested that the constant in the heat transfer equation be 0.25 for bored shells and 0.22 for unbored shells. For wide tube pitch he recommended that

$$C = 0.19\ (d_e)^{0.6}$$

In all cases C is less than that obtained for pure crossflow

relations and is thus intended to account for various leakages.

In two papers T. Tinker outlined a method for analyzing the various shell-side streams shown in figure 3. In the former paper (12) he set up several empirical relations to determine the pressure drop of the various streams. By apportioning the flows so that their pressure drops were equal over a baffle spacing, he was able to determine the ratios of each to the crossflow stream. An effective cross-flow area (A_{eff}) is then defined as,one that would accomodate all the streams at the same mass velocity as the crossflow component gives through the actual crossflow zone.

Then $$A_{eff} = A_c \left(1 + \frac{Q_a}{Q_b} + \frac{Q_c}{Q_b} + \frac{Q_e}{Q_b}\right)$$

Where Q denotes the relative mass flows and the subscripts refer to the various streams shown in figure 3. Then

$$G_{eff} = \frac{\text{Total mass flow}}{A_{eff}}$$

and $$Re_{eff} = \frac{G_{eff}\, D}{\mu}$$

with $$J_h = \frac{Nu}{P_r^{\frac{1}{3}} \left(\frac{\mu}{\mu_w}\right)^{0.14}} = 0.58 \left(Re_{eff}\right)^{0.543}$$

for the crossflow area in the range of effective Reynolds' number above 1,000. The total heat transfer coefficient, for a baffle spacing is determined by reducing the crossflow

coefficient by an empirical multiplier which decreases with increasing baffle cut.

Great difficulty is encountered when this first method is used, since the coefficients in the various flow stream equations are variables which are dependent on the characteristics of other flow streams. This results in a trial and error method to apportion the various leakage and main stream flows.

In Tinker's later paper (13) he greatly simplified this method. Heat transfer in the window area was assumed to depend on Donohue's geometric-mean mass velocity.

In order to obtain an overall mean heat transfer coefficient from a crossflow relationship, he reversed Bergelin et al's method.

$$h_o S_t = h_c S_t - h_c S_w + h_w S_w$$

but $$h_c \approx \frac{c}{(A_c)^{0.6}}$$

and $$h_w \approx \frac{c}{(A_m)^{0.6}}$$

Defining an average flow area, A_v, on which to base a weighted average mass velocity for the whole baffle section, he proposed $h_o \approx \frac{c}{(A_v)^{0.6}}$

$$\text{then } \frac{1}{(A_v)^{0.6}} = \left[\frac{S_t - S_w}{(A_c)^{0.6}} + \frac{S_w}{(A_m)^{0.6}}\right] \frac{1}{S_t}$$

Once again it was necessary to apportion the various streams in order to determine an effective mass velocity for

heat transfer. This time the relationships were based on the shell diameter to baffle spacing ratio, the shell diameter to tube pitch ratio, the pitch ratio, and the baffle clearances (all of which remain constant for a given exchanger). From these a multiplying factor, F_h, is determined. Then

$$G_{eff} = \frac{\text{mass flow}}{A_v} \times F_h$$

Then a heat transfer Reynolds' number is calculated. An average shell-side heat transfer coefficient is then obtained from the expression given in his first paper.

Results from Tinker's methods have been most accurate. However, verification of the behaviour of the various flow streams is required as well as the relationship between window and crossflow heat transfer coefficients.

Results and Discussion

Local Coefficients

The first step in analyzing the results was to make individual plots of the local heat transfer coefficients for each flow rate and baffle spacing. Crossflow zone coefficients are represented, in appendix 11, by figure 18 to figure 32. Entry and exit window zone coefficients are combined and shown in figure 33 to figure 47. It was decided to identify each flow rate by the usual heat exchanger crossflow Reynolds' number, Re_c. Figure 13 codifies crossflow and window zone row numbers, probe positions and test section terminology used in these charts and following discussion.

Analysis revealed that the crossflow region can be divided into two sub-zones: flow region and dead region. At all baffle spacing, and all rows in the former sub-zone, maximum heat transfer coefficients tended to be located at probe positions nearest the right hand baffle in figure 13. Lower coefficients were obtained to the left of these positions. This corresponds to the results obtained by Gurashankariah and Knudsen (10) in their crossflow area. However, in the dead region, which corresponds in location to their eddy flow area, heat transfer rates dropped off rapidly. The absence of baffle-tube hole leakage obviously eliminated any heat transfer due to orifice flow in the region adjacent to the upstream baffle.

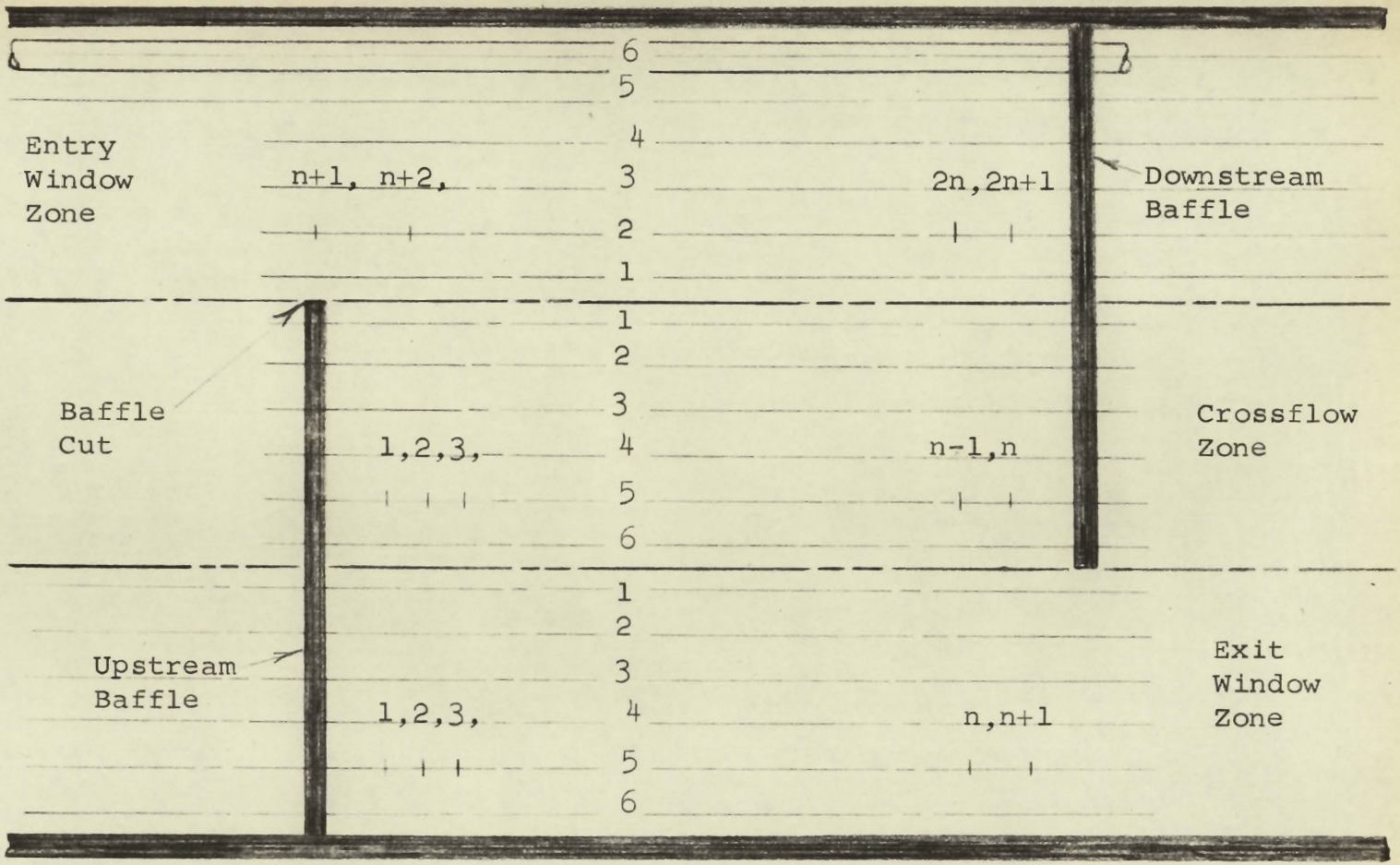

FIGURE 13: TEST SECTION TERMINOLOGY AND PROBE LOCATIONS

In each row of the window-zone maximum coefficients were obtained near probe position n + 1, adjacent to the baffle cut. Heat transfer rates continued to decrease as the probe was moved to the opposite side of the test section, in both the entry and exit window regions. This also corresponds to Gurashankariah and Knudsen's results. However, minimum rates were obtained near the baffle since leakage had been eliminated.

Generally, for corresponding probe positions in the window zone, heat transfer decreased from the first row to the sixth. This result is probably due to three factors. First of all the portion of the overall flow penetrating the tube-bundle in the window zone was reduced, row by row, from the baffle cut to the shell. Due to the fact that the flow must turn in the window, its angle of impingement, at corresponding probe positions, must be closer to cross flow at lower row numbers. Finally the effect of turbulence, caused by the baffle, would be greatest at those positions nearest the baffle cut.

One exception to the above general condition should be noted. At 60 per cent and 100 per cent baffle spacing, heat transfer rates decreased to minimum values at probe positions immediately downstream from the left hand baffle on the first row inside the entry window zone. This behaviour was more pronounced at the widest baffle spacing and tended to increase

at higher flow rates. This phenomenon supports the theory that flow through a baffle entry is similar to flow over a weir. The vena contracta formed by such flow creates a void immediately downstream from entry. At the smallest baffle spacing the proximity of the next baffle interferes with this type of flow, and therefore no sharp decrease in heat transfer was obtained.

Crossflow-zone correlation

The presence of the dead region in the crossflow zone quantitatively confirms the existence of the turbulent wake reported in the photographic studies of Gunter et al (5). This complicates considerably the task of obtaining a correlation for the crossflow zone.

It was therefore decided to determine the average heat transfer coefficients for the two crossflow sub-zones separately. Since there is practically no net flow in the dead region it was decided to base the mass velocity on the narrowest cross-section area of the flow region, in determining comparative Reynolds' numbers (Re_f).

Plots of the heat transfer factor, J_h, for two sub-zones are shown in figure 14. They reveal that the average coefficients in the flow region can be correlated by a single curve which is approximately 20 per cent lower than Grimison's correlation for pure cross flow.

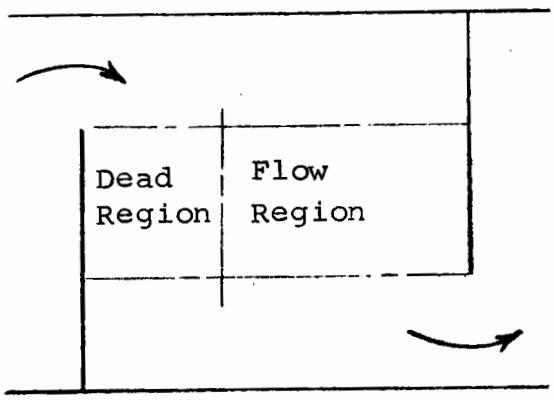

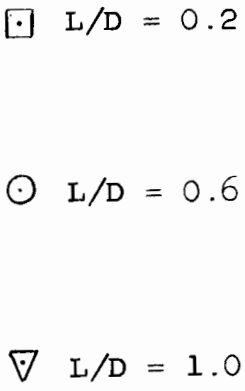

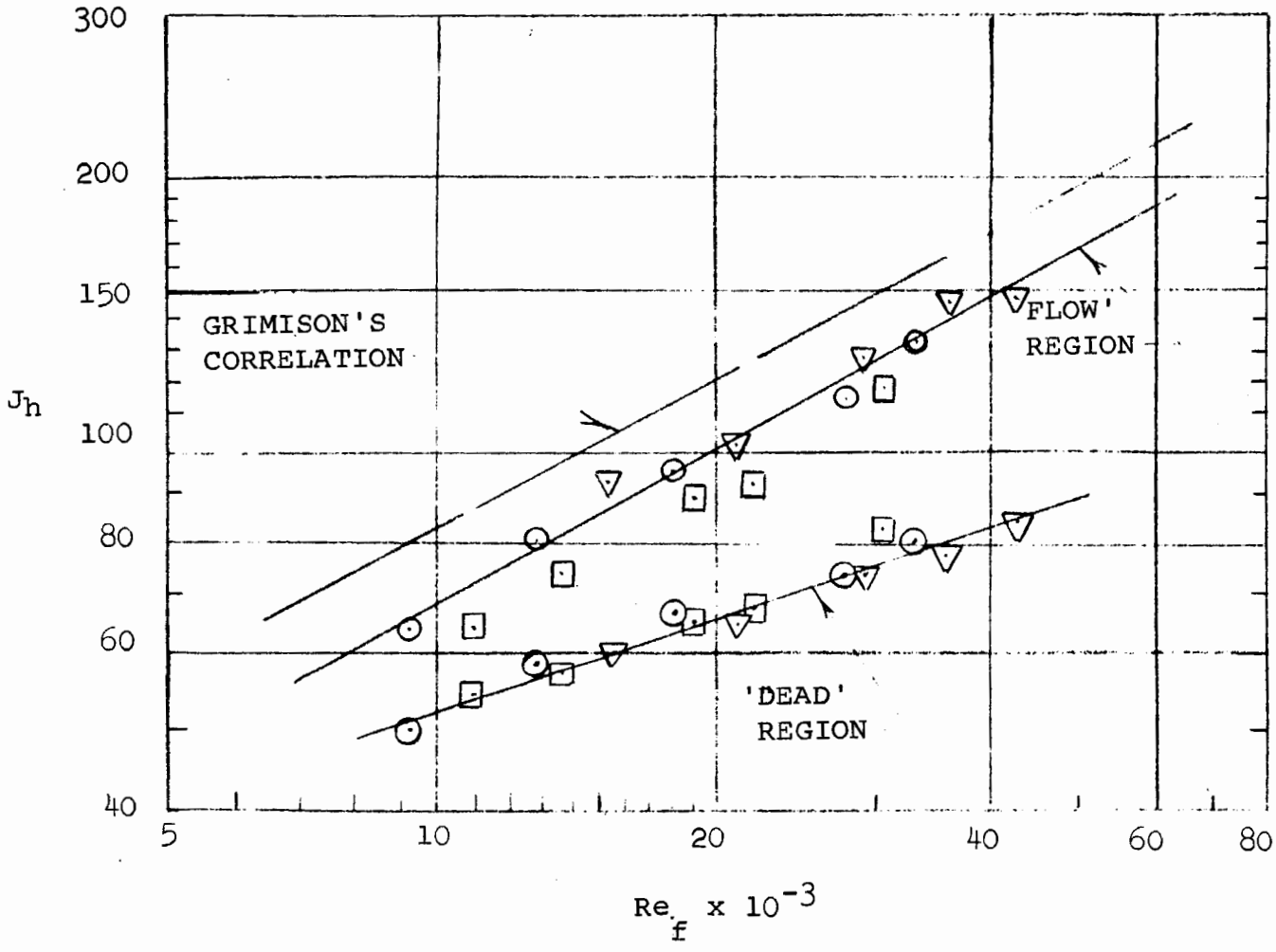

FIGURE 14: CROSSFLOW SUB-ZONE HEAT TRANSFER RATES.

Part of this discrepancy is due to the assumption that no flow takes place in the dead region, and the Reynolds' numbers used in these plots assume higher velocities than those actually occurring. From the experimental procedure it was expected that the results could be about 10 per cent lower than the actual values.

In the dead region heat transfer rates are much lower and considerably less sensitive to changes in flow rates. Since the average coefficient in the whole crossflow zone is a weighted mean of the two sub-zones, the relative insensitivity of the dead region coefficients will tend to decrease the Reynolds' number exponent, a, with increased area ratio, A_r, in the usual heat transfer expression

$$J_{h_c} = \frac{Nu_c}{Pr^{\frac{1}{3}} \left(\frac{\mu}{\mu_w}\right)^{0.14}} = C\ Re_c^{a} \qquad (1)$$

It can also be expected that the constant, C, will be influenced by the relative size of the dead region, since the mass velocity in the flow region would be much greater than the average used in determining Re_c. Plots of average J_h factors for the crossflow zone are shown in figure 15 and three curves obtained confirm these expectations.

Thus, neither C nor a in equation (1) are constants and must be expressed as functions of the area ratio, A_r. The heat transfer equation can be rewritten

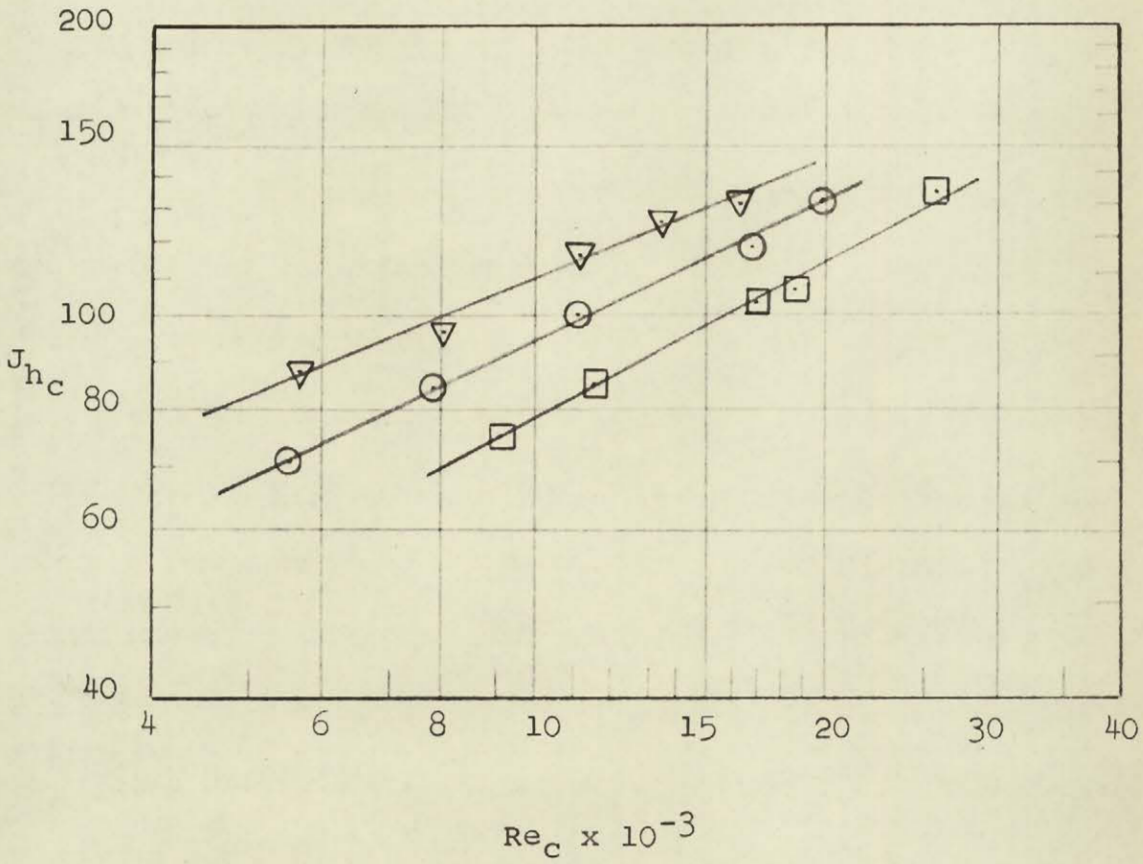

⊡ L/D = 0.2

⊙ L/D = 0.6

▽ L/D = 1.0

FIGURE 15: AVERAGE CROSSFLOW ZONE HEAT TRANSFER RATES

$$J_{h_c} = f_1(A_r)\, Re_c^{\,f_2(A_r)}$$

Analysis of the experimental results reveal that

$$f_1(A_r) = 0.868\, A_r^{\,0.780}$$

and $$f_2(A_r) = 0.490\, A_r^{\,-0.126}$$

The heat transfer equation for the crossflow zone then becomes

$$J_{h_c} = 0.868\, A_r^{\,0.780}\, Re_c^{\,0.490\, Ar^{-0.126}} \qquad (2)$$

which expresses the experimental results within $\pm$ 4 per cent.

Window zone correlation

Due to the dead regions in the corners formed by the baffles and the shell wall, and the effect of the vena contracta, plots of average window zone heat transfer factors, J_{hw}, result in three distinct curves for the three baffle spacings as shown in figure 16. Therefore an equation, similar to the one derived for the crossflow zone, was required to correlate window zone heat transfer.

Analysis revealed that for the window

$$f_1(A_r) = 0.721\, A_r^{\,1.01}$$

and $$f_2(A_r) = 0.490\, A_r^{\,-0.126}$$

Therefore the correlating expression for the window zone can be written as

$$J_{h_w} = 0.721\, A_r^{\,1.01}\, Re_c^{\,0.490\, A_r^{-0.126}} \qquad (3)$$

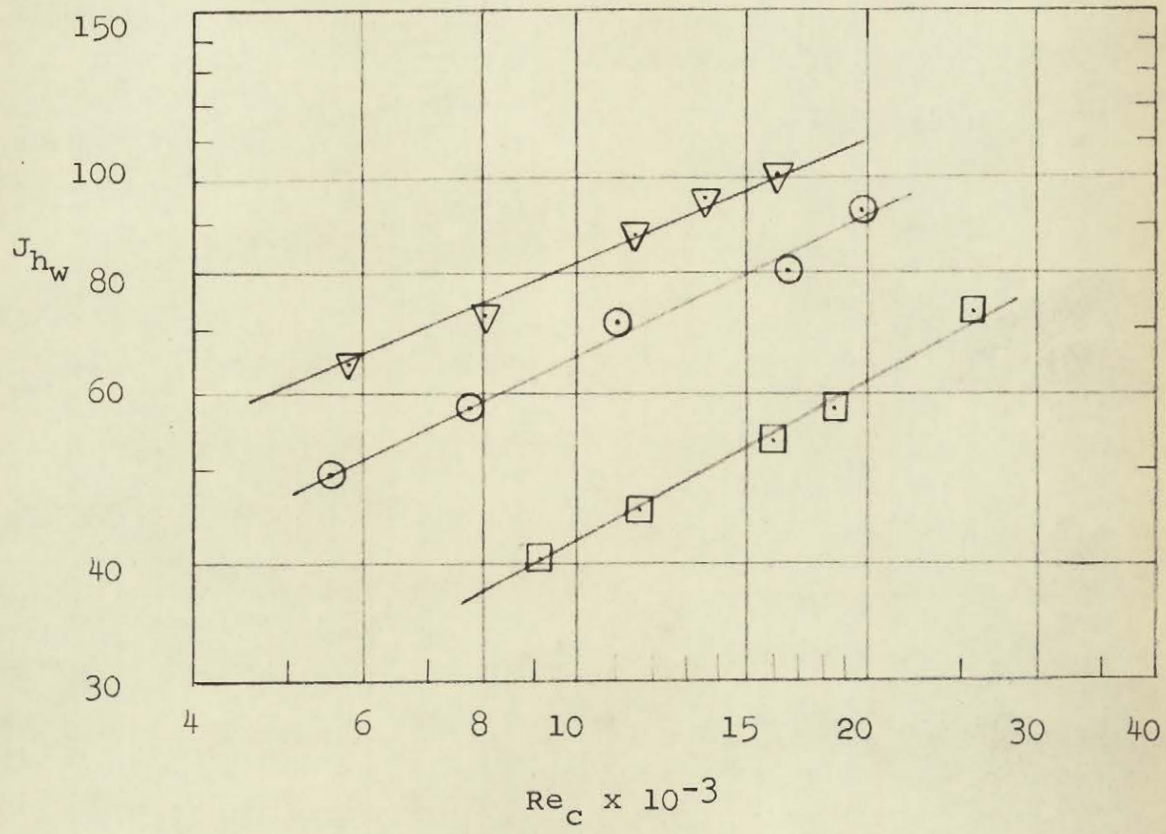

⊡ L/D = 0.2

⊙ L/D = 0.6

▽ L/D = 1.0

FIGURE 16: AVERAGE WINDOW ZONE HEAT TRANSFER RATES

Although this expression is similar to the one obtained for the crossflow zone, certain differences are noted. Heat transfer rates have a much greater variation with changing area ratio, A_r. In order to obtain an expression with the same degree of dependency as that used for the crossflow zone, equation (3) must be rewritten as

$$J_{h_w} \simeq 0.721\, A_r^{1.01}\, Re_c^{0.5} \qquad (4)$$

This is possible as the variation in $f_2\,(A_r)$ is from 0.459 to 0.563. Then

$$A_r = \frac{A_c}{A_w}$$

$$\text{and } Re_c = \frac{G_c\, d}{\mu}$$

$$\text{but } Re_m = \frac{(G_c\, G_w)^{0.5}}{\mu}$$

$$\text{Therefore } Re_c = Re_m \frac{G_c}{(G_c\, G_w)^{0.5}} = Re_m \left(\frac{A_w}{A_c}\right)^{0.5}$$

$$\text{hence } Re_c = Re_m\, Ar^{-0.5} \qquad (5)$$

Substituting (5) in equation (4) yields

$$J_{h_w} \simeq 0.721\, A_r^{0.76}\, Re_m^{0.5}$$

The correlating equation for the window zone can be rewritten as

$$J_{h_w} = 0.721\, A_r^{0.76}\, Re_m^{0.490}\, A_r^{-0.126} \qquad (6)$$

This expression, with about the same degree of dependency on the area ratio as the one obtained for the crossflow zone, yields heat transfer coefficients which are within $\pm$ 4.5 per cent of the experimental results.

Interpretation of Results

In order to compare crossflow and window heat transfer rates more readily, it is desirable to modify the heat transfer equations so that

$$J_h' = C\ R_e^{\ a}$$

where J_h' is a modified heat transfer factor and is a function of the area ratio, A_r. The exponents of the area ratio term in equations (2) and (6) can be averaged at 0.770 while maintaining correlating expressions within experimental accuracy. These equations are of the form

$$J_h = C_1\ (A_r)^{0.770}\ R_e^{\ 0.490}\ A_r^{\ -0.126} \qquad (7)$$

From this a modified heat transfer was obtained in appendix 1. Then for the crossflow zone

$$J_{h_c}' = \left(\frac{J_{h_c}}{A_r^{\,n}}\right) A_r^{0.126} = 0.868\ Re_c^{\ 0.490} \qquad (8)$$

$$\text{where } n = 0.770 - \frac{0.018}{A_r^{0.126}} \qquad (8a)$$

and for the window zone

$$J_{h_w}' = \left(\frac{J_{h_w}'}{A_r^{\,n}}\right) A_r^{0.126} = 0.721\ Re_m^{\ 0.490} \qquad (9)$$

$$\text{where } n = 0.770 - \frac{0.041}{A_r^{0.126}} \qquad (9a)$$

Experimental results, expressed as modified heat transfer factors, are plotted in figure 17 for the

crossflow and window zones against crossflow and geometric mean, Reynolds' numbers respectively. Two correlating curves are obtained which confirm the previous analysis.

The most significant thing about this result is that the exponents of the Reynolds' number is identical in equations 8 and 9. In fact both expressions would be the same except for the value of the constant in the window zone correlation which is some 17 per cent below the crossflow value. This confirms experimentally that, while heat transfer in the crossflow zone can be correlated to crossflow Reynolds' numbers, the coefficients in the window zone should be correlated to a Reynolds' number based on the geometric-mean mass velocity.

It is felt that this conclusion can be safely extended to conventional heat exchangers. Although leakages would cause changes in the constants and exponents of the correlations, basic flow patterns would remain the same.

The correlating factor, A_r, is primarily a result of the great dependence of the average coefficients on the size of the dead region. With the introduction of baffle-tube-hole leakage the major portion of the dead regions, immediately downstream of the baffle and in the baffle-shell corner, would be eliminated. It is possible that under these conditions A_r would cease to be a correlating factor.

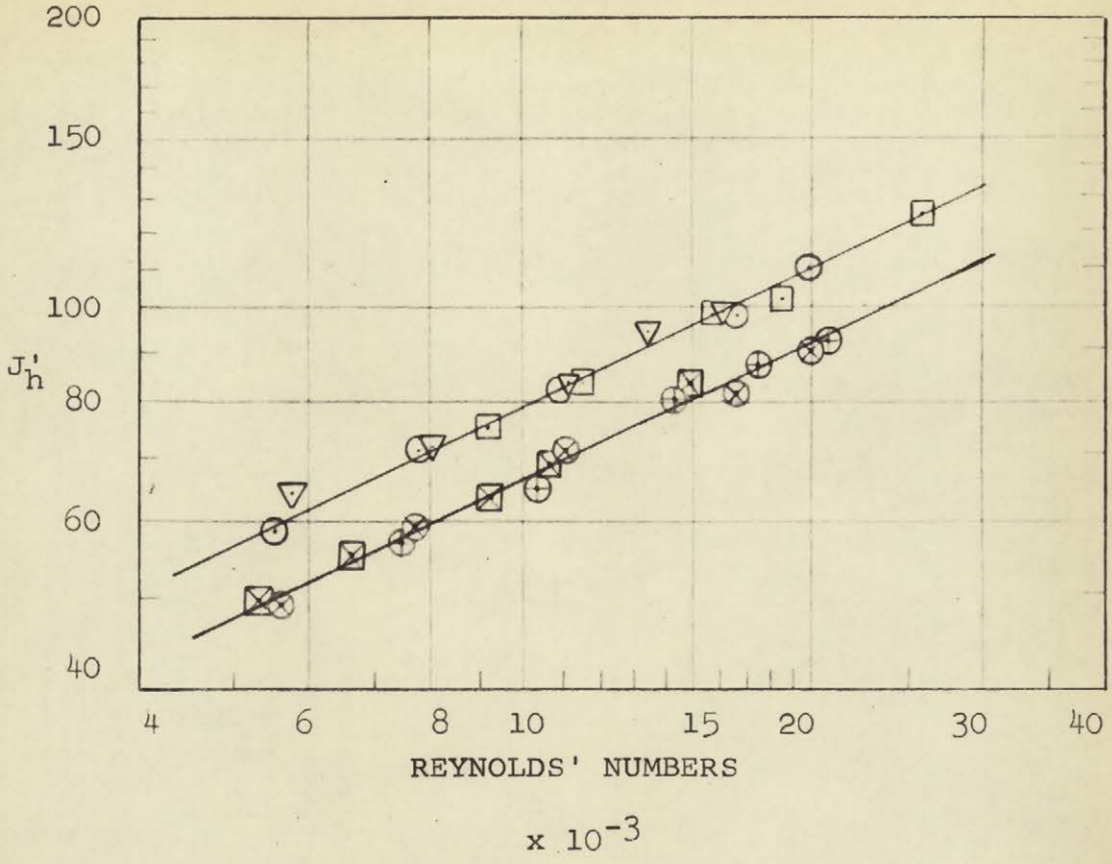

CROSSFLOW

⊡ L/D = 0.2

⊙ L/D = 0.6

▽ L/D = 1.0

WINDOW ZONE

⊠ L/D = 0.2

⊘ L/D = 0.6

⊕ L/D = 1.0

FIGURE 17: CORRELATION OF CROSSFLOW AND WINDOW ZONE HEAT TRANSFER FACTORS.

The 17 per cent discrepancy, between the crossflow and window zone correlating curves, suggests that Tinker's (13) use of the same correlating equation, for both zones, might lead to unsafe design. It should be pointed out, however, that in cylindrical commercial exchangers the number of tubes is much greater in rows nearest the baffle cut than in those at the top of the baffle window. Hence the low local coefficients prevailing at the top of the window, in a commercial exchanger, would have a smaller effect on the average value than in a rectangular model. Also the increase of heat transfer, due to leakage, is likely to be greater in the window than in the crossflow dead region, since there is a greater pressure drop available to drive the flow through the various clearances. However, additional research is required to verify the complete disappearance of this difference in commercial cylindrical exchangers.

Recommendations

The work described in this thesis can be considered only as a first step towards a detailed analysis of shell-side characteristics in segmental baffle heat exchangers. Further idealized studies are required.

Experiments, carried out with additional baffle spacings and various window openings, are necessary to verify the correlations obtained or to determine how they should

be modified. The introduction of various leakages, one at a time and collectively, would permit authentication or modification of Tinker's methods for analyzing commercial exchangers. Finally, measurements of local heat transfer coefficients, in typical commercial heat exchangers, would reveal any differences between characteristics due to flow in a cylindrical shell and that in a rectangular model.

Conclusions

From the idealized conditions under which this experiment was carried out it is concluded that the crossflow region of a leak-proof heat exchanger can be divided into two sub-zones: dead region and flow region. The size of these sub-zones is a function of the area ratio, A_r, and thus the average heat transfer coefficient is also a function of A_r.

A single correlation for various area ratios was obtained by deriving a modified heat transfer factor, J_h'. Heat transfer rates for the crossflow zone can be correlated by $J'_{h_c} = 0.868\ Re_c^{0.490}$, while window zone coefficients can be expressed by $J'_{h_w} = 0.721\ Re_m^{0.490}$, to within $\pm$ 5 per cent. This verifies experimentally that, while Re_c is the correct parameter for the crossflow zone correlation, Re_m should be used for the window zone.

Bibliography

1. Flow Measurement - British Standard Code, B.S. 1042. British Standards Institution, London, 1943

2. Heat and Mass Transfer - E.R.G. Eckert and R.M. Drake. 2nd Edition, McGraw-Hill, 1959.

3. Die Berechnung der Warmeuberganges in der Laminaren Grenzschicht Umstromter Koerper - E.R.G. Eckert. VDI Forschungsheft, p.416, 1942.

4. Heat Transmission - W.H. McAdams. 3rd Edition, McGraw-Hill, p.259, 1954.

5. Flow Past Two-Dimensional Baffles - A.Y. Gunter, H.R. Sennstrom and S. Kopp. Paper 47-A-103, A.S.M.E. meeting, Atlantic City, N.J., 1947.

6. Correlation and Utilization of Flow Resistance and Heat Transfer for Crossflow of Gases over Tube-Banks - E.D. Grimison, A.S.M.E. Transactions, PRO-S9-8, vol.59, pp. 583-594, 1937.

7. The Influence of Angle of Impingement on Heat Transfer Coefficients and Pressure Drops for Flow of Air over a Tube-Bank - G.A. Shaw. Master's Thesis, McGill University, 1956.

8. Heat Transfer in Tube-Bundles as a Function of the Angle of Impingement - A.P. Ornatski. Sovetskoe Kotloturbostroeni, vol.2, p.418, 1940.

9. Heat Transfer and Fluid Friction during Flow across Banks of Tubes, V-A study of a Cylindrical Baffled Exchanger without Internal Leakage - O.P. Bergelin, G.A. Brown and A.P. Colburn. A.S.M.E. Transactions, vol.76, pp.841-850, 1954.

10. Local Shell-Side Heat Transfer Coefficients in the Vicinity of Segmental Baffles in Tubular Heat Exchangers - M.S. Gurashankariah and J.G. Knudsen, paper 19, 2nd. National Heat Transfer Conference. A.I.Ch.E. - A.S.M.E., Chicago, Ill., 1958.

11. Heat Transfer and Pressure Drop in Heat Exchangers - D.A. Donohue.
Industrial and Engineering Chemistry, vol.41, pp. 2499-2511, 1949.

12. Shell-Side Characteristics of Shell and Tube Heat Exchangers - T. Tinker.
Proceedings of General Discussion on Heat Transfer. I. Mech. E. - A.S.M.E., pp.89-116, 1951.

13. Shell-Side Characteristics of Shell and Tube Heat Exchangers - A simplified rating system for commercial exchangers - T. Tinker.
A.S.M.E. Transactions, vol.80, pp.36-52, 1958.

Appendix 1

Derivation of Modified Heat Transfer Factor.

Experimental results in both the crossflow and window zone can be correlated by the following type of equations

$$J_h = C_1 A_r^{0.770} Re^{0.490} A_r^{-0.126} \qquad (7)$$

The desired form of the correlation is

$$J_h' = C\ Re^{a}$$

This form can be obtained if

$$J_h = C_2 A_r^{-0.126} A_r^{n} Re^{0.490 A_r^{-0.126}} \qquad (10)$$

then $$J_h' = \left(\frac{J_h}{A_r^{n}}\right)^{A_r^{0.126}} = C_2 Re^{0.490}$$

If equation (10) is to be identical to equation (7) then

$$C_1 A_r^{0.770} = C_2 A_r^{-0.126} A_r^{n}$$

For this to hold for all values of A_r (including $A_r = 1$)

$$C_1 = C_2^{A_r^{0.126}}$$

Therefore $$C_1 A_r^{(0.770-n)} = C_1^{A_r}$$

Taking logarithms

$$\log C_1 + (0.770 - n) \log A_r = A_r^{-0.126} \log C_1$$

Appendix 1

Multiplying by $A_r^{0.126}$ and transposing

$$A_r^{0.126} = \frac{1 + (n-0.770)A_r^{0.126}\log A_r}{\log C_1} \qquad (11)$$

The left hand side of (11) can be expanded by the exponential series so that

$$A_r^{0.126} = 1 + 0.126 \log A_r + \frac{(0.126 \log A_r)^2}{2!}$$

$$+ + + \frac{(0.126 \log A_r)^x}{x!} + + +$$

For the range of values of A_r used in this experiment, as well as those usually found in commercial exchangers, this series converges so rapidly that all terms beyond the second can be neglected with less than 1 per cent error. Thus if

$$1 + 0.126 \log A_r = 1 + \frac{(n-0.770)A_r^{0.126}\log A_r}{\log C_1}$$

Equation (10) can be used as the correlating expression provided

$$n = 0.770 + \frac{0.126 \log C_1}{A_r^{0.126}}$$

Thus for the crossflow zone

$$n = 0.770 - \frac{0.018}{A_r^{0.126}} \qquad (8a)$$

and for the window zone

$$n = 0.770 - \frac{0.041}{A_r^{0.126}} \qquad (9a)$$

Appendix II

Local Heat Transfer Coefficients.

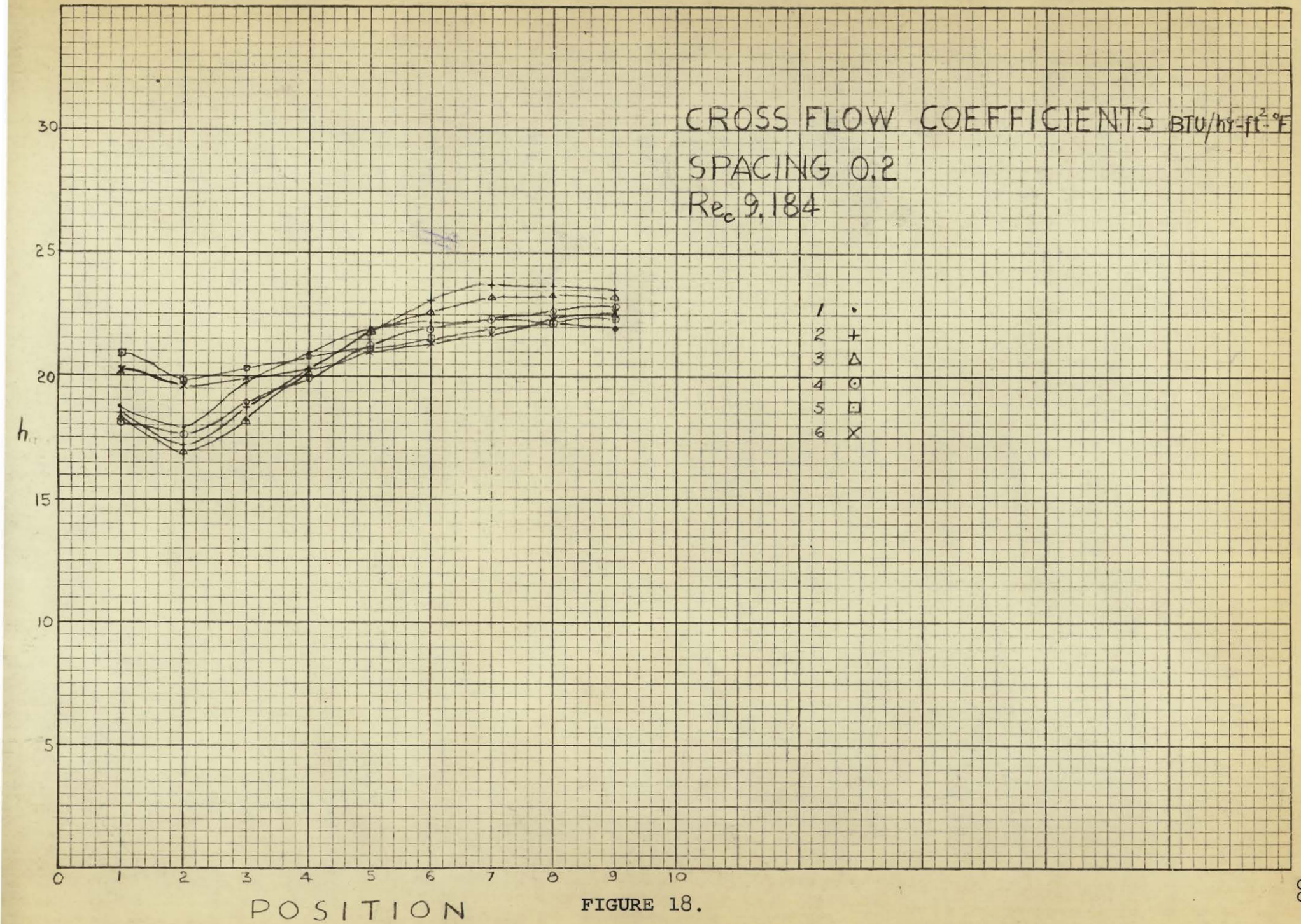

FIGURE 18.

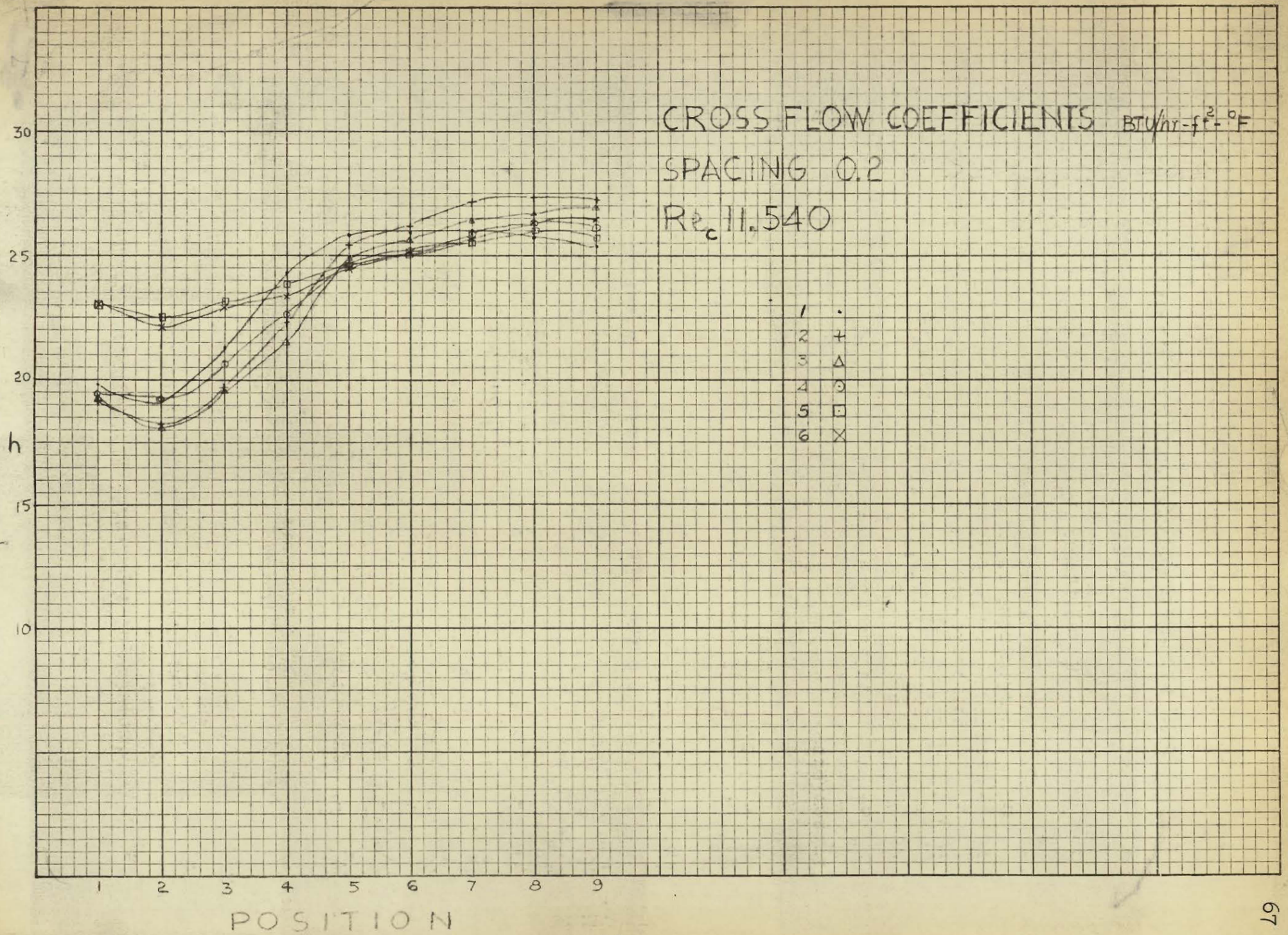

FIGURE 19.

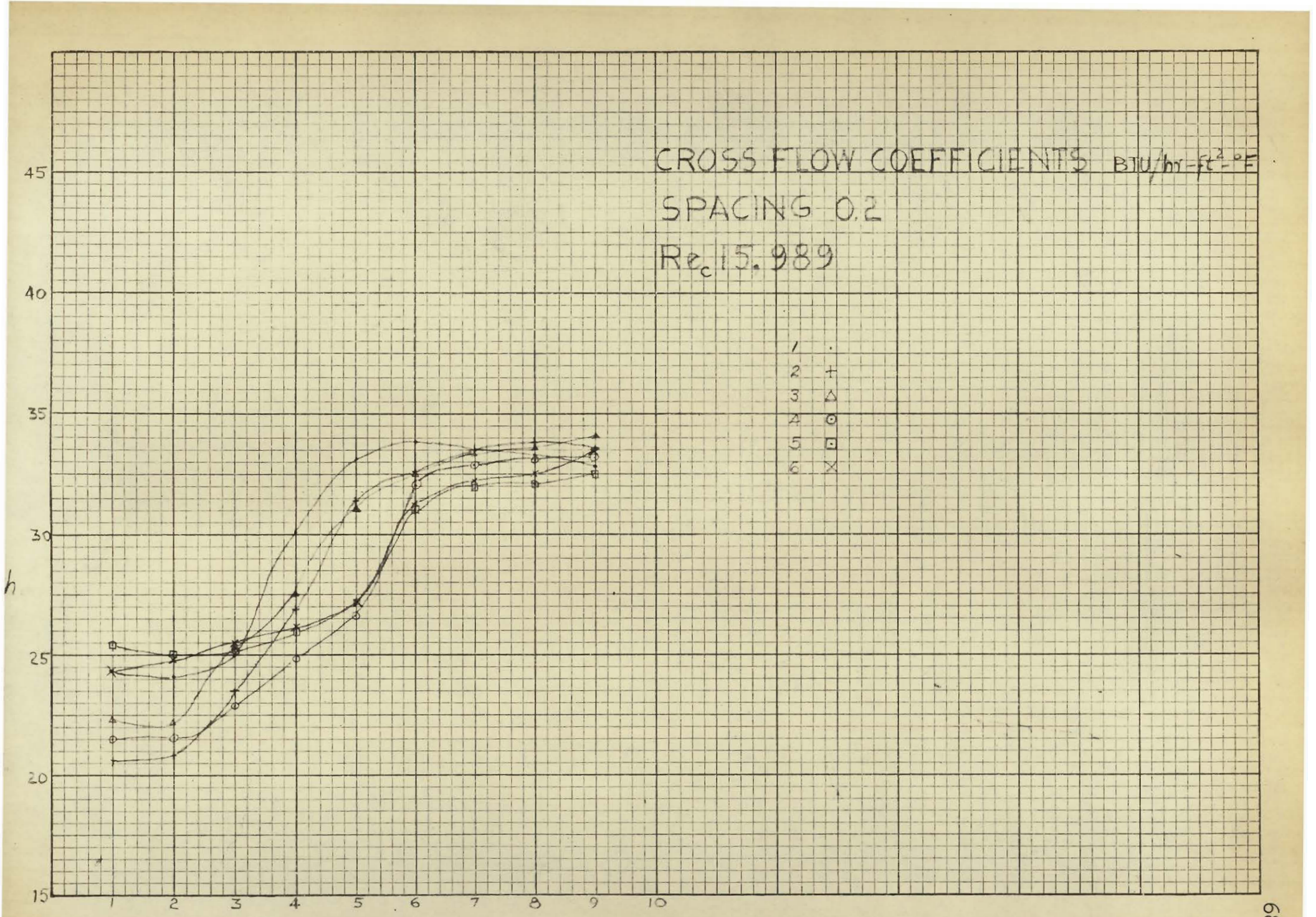

FIGURE 20.

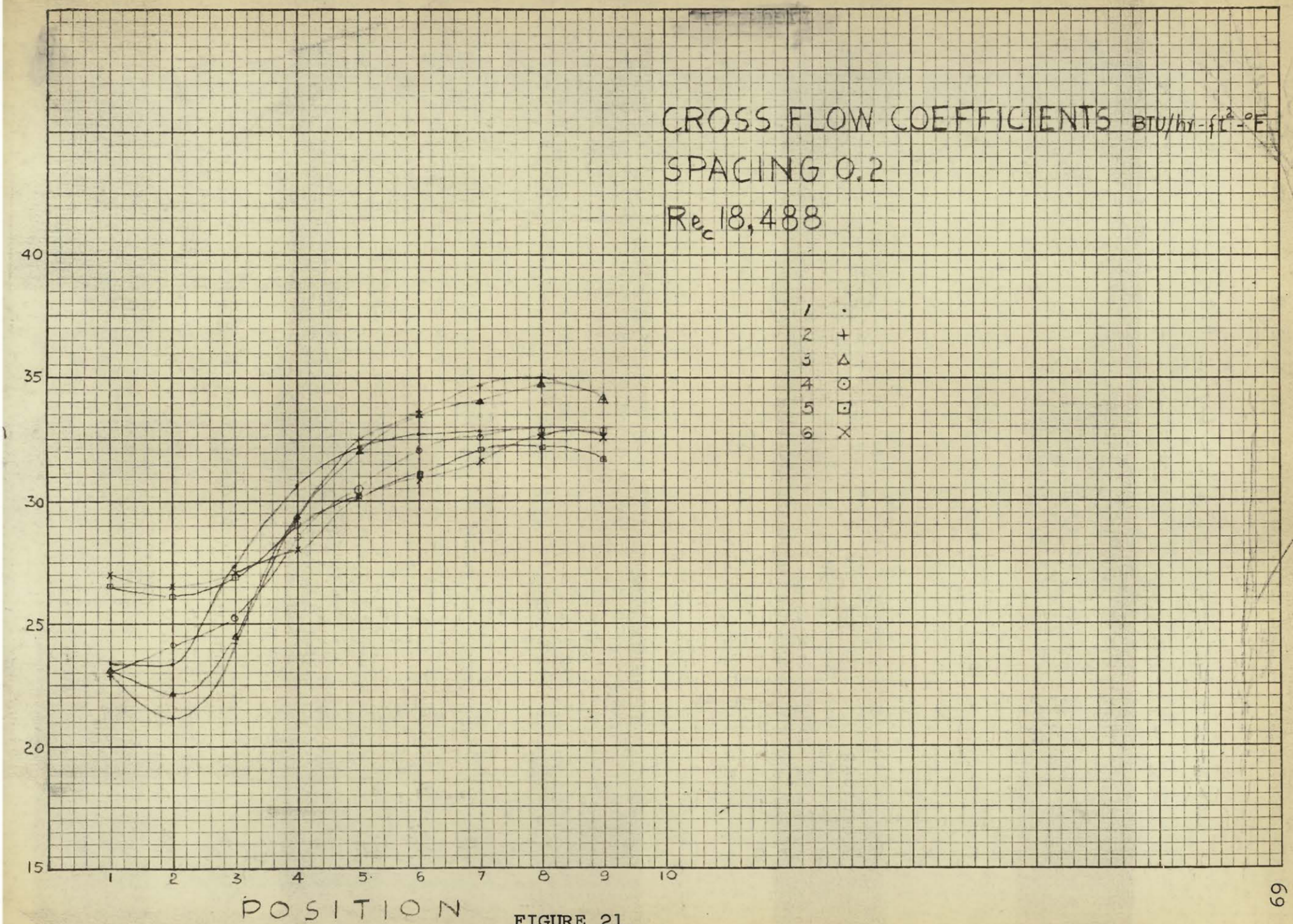

FIGURE 21.

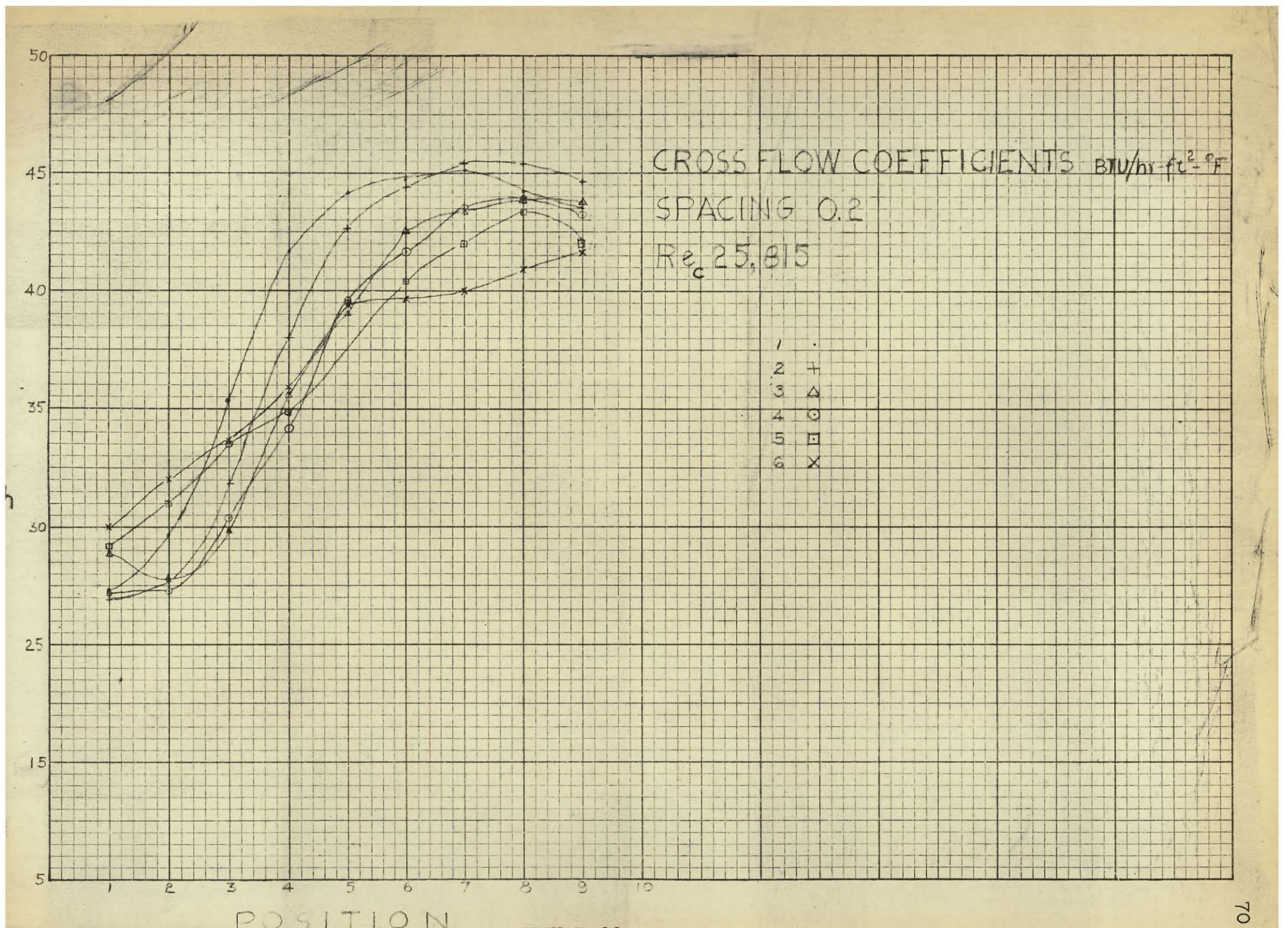

FIGURE 22 .

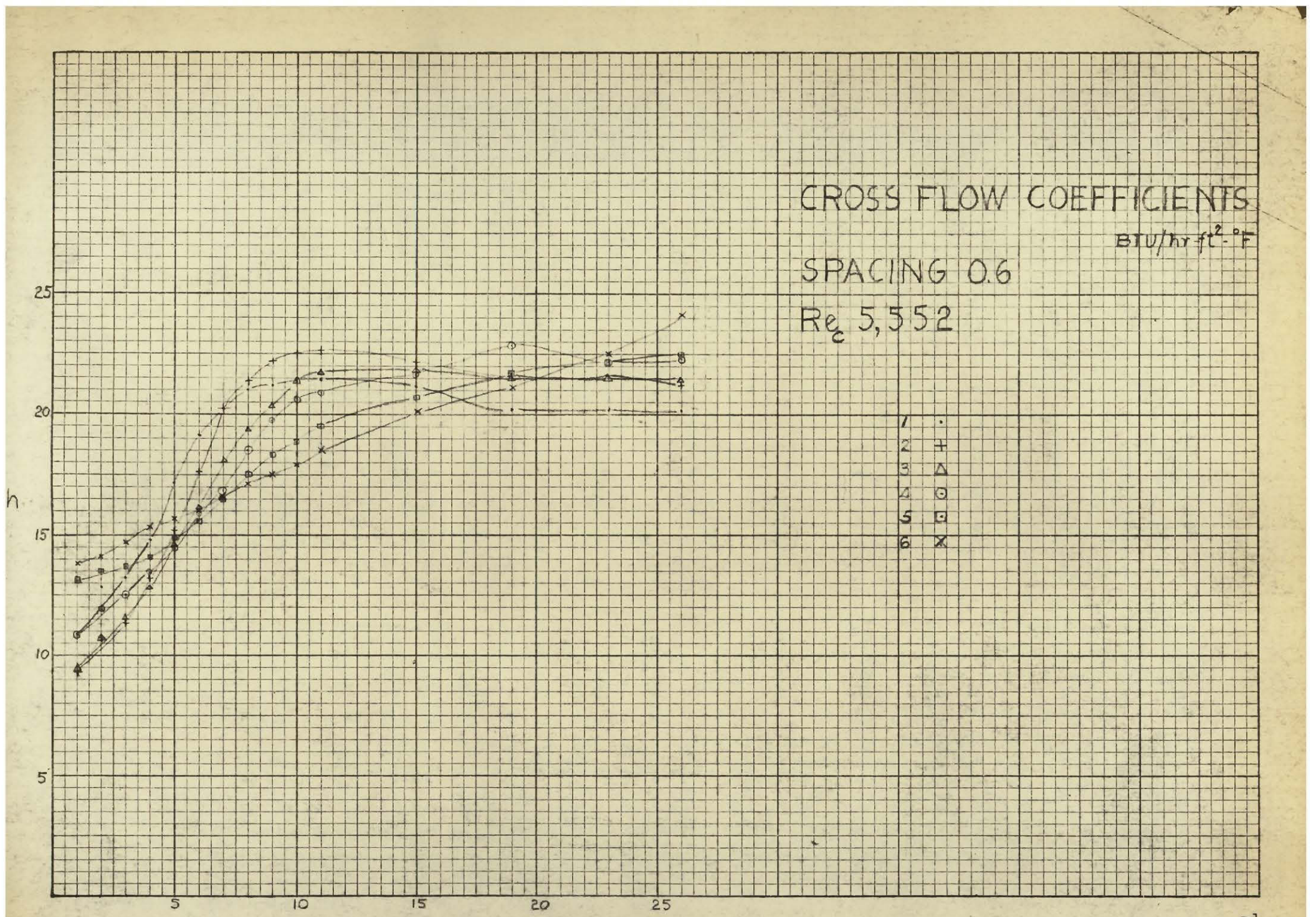

FIGURE 23.

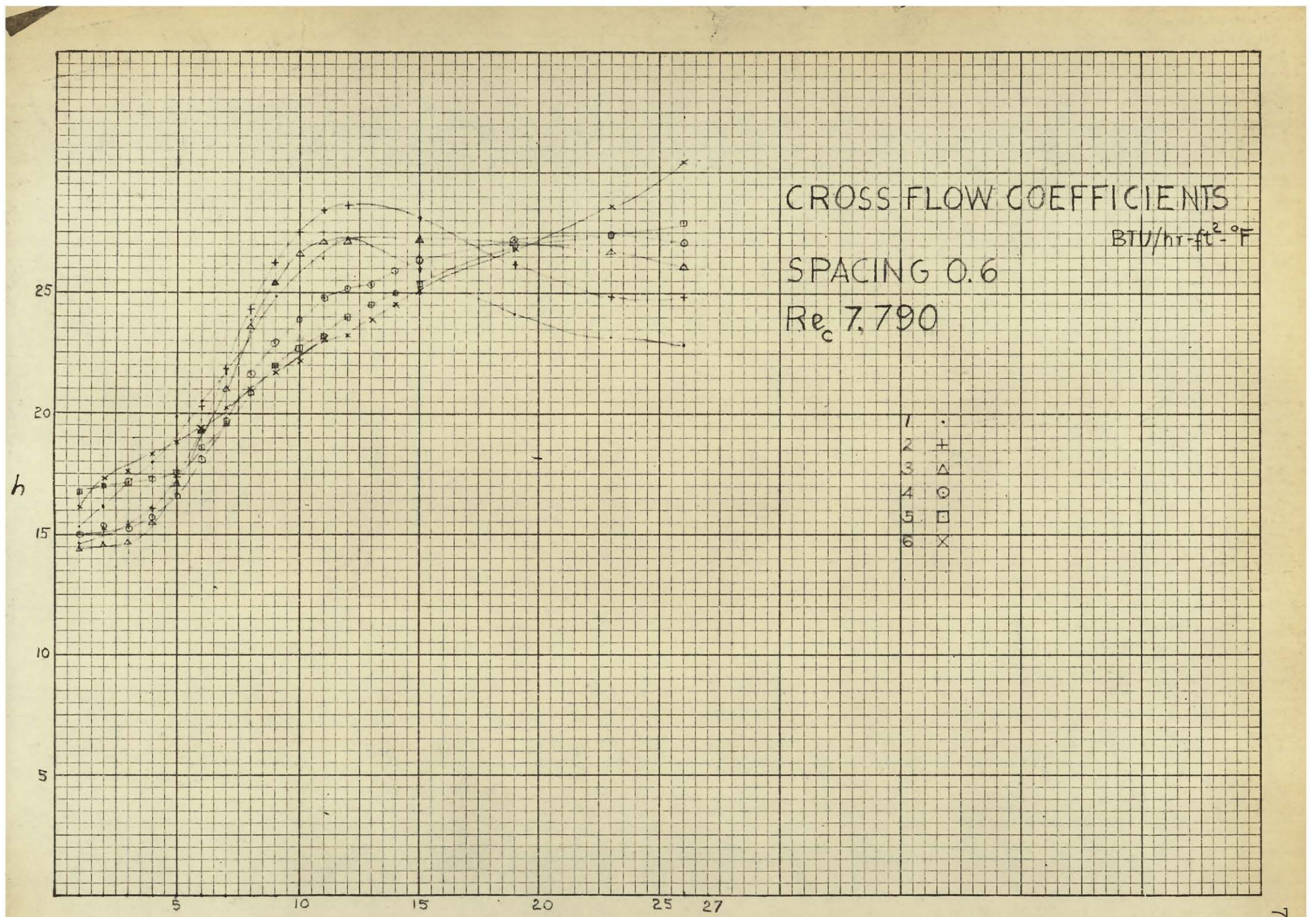

FIGURE 24.

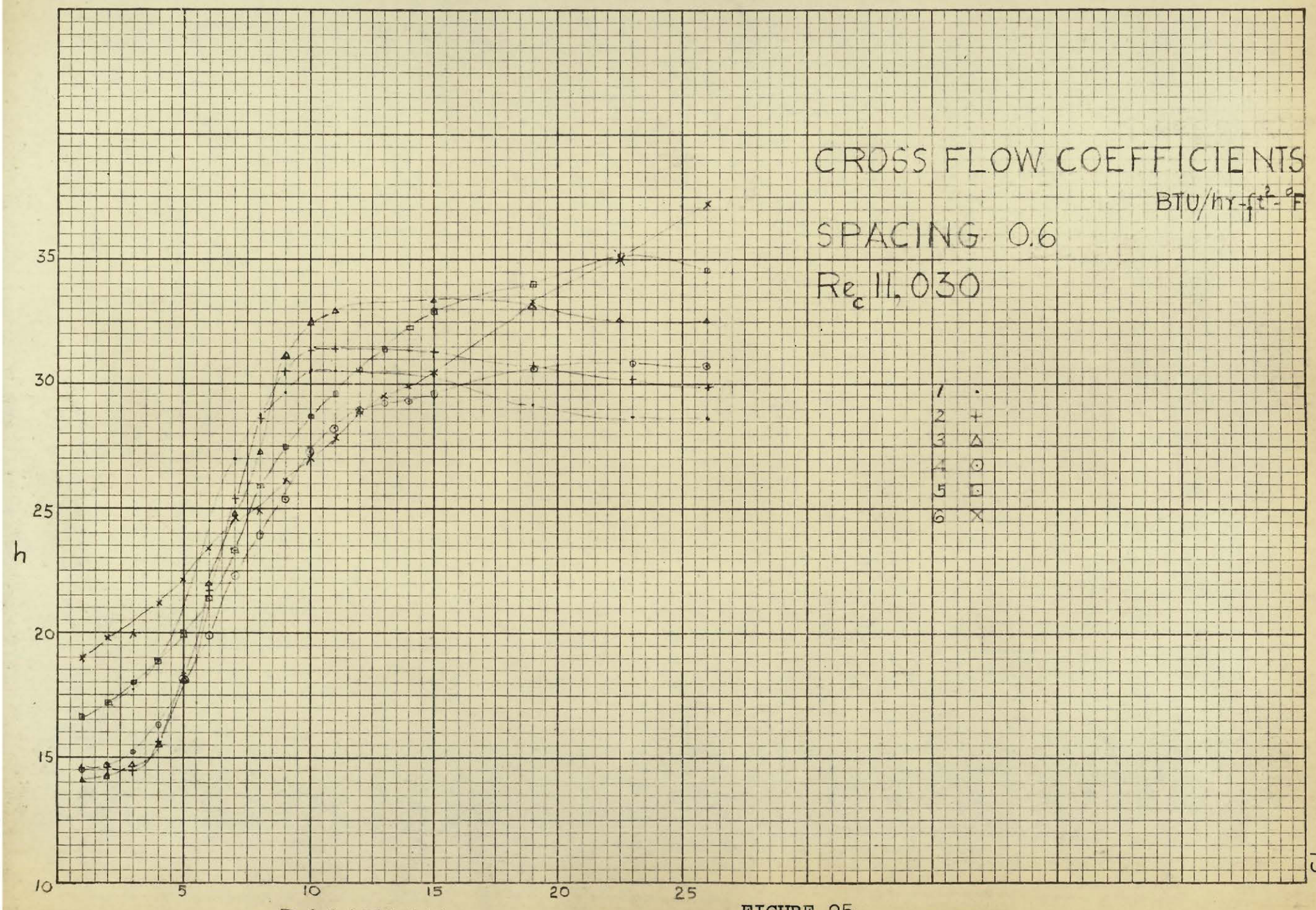

FIGURE 25.

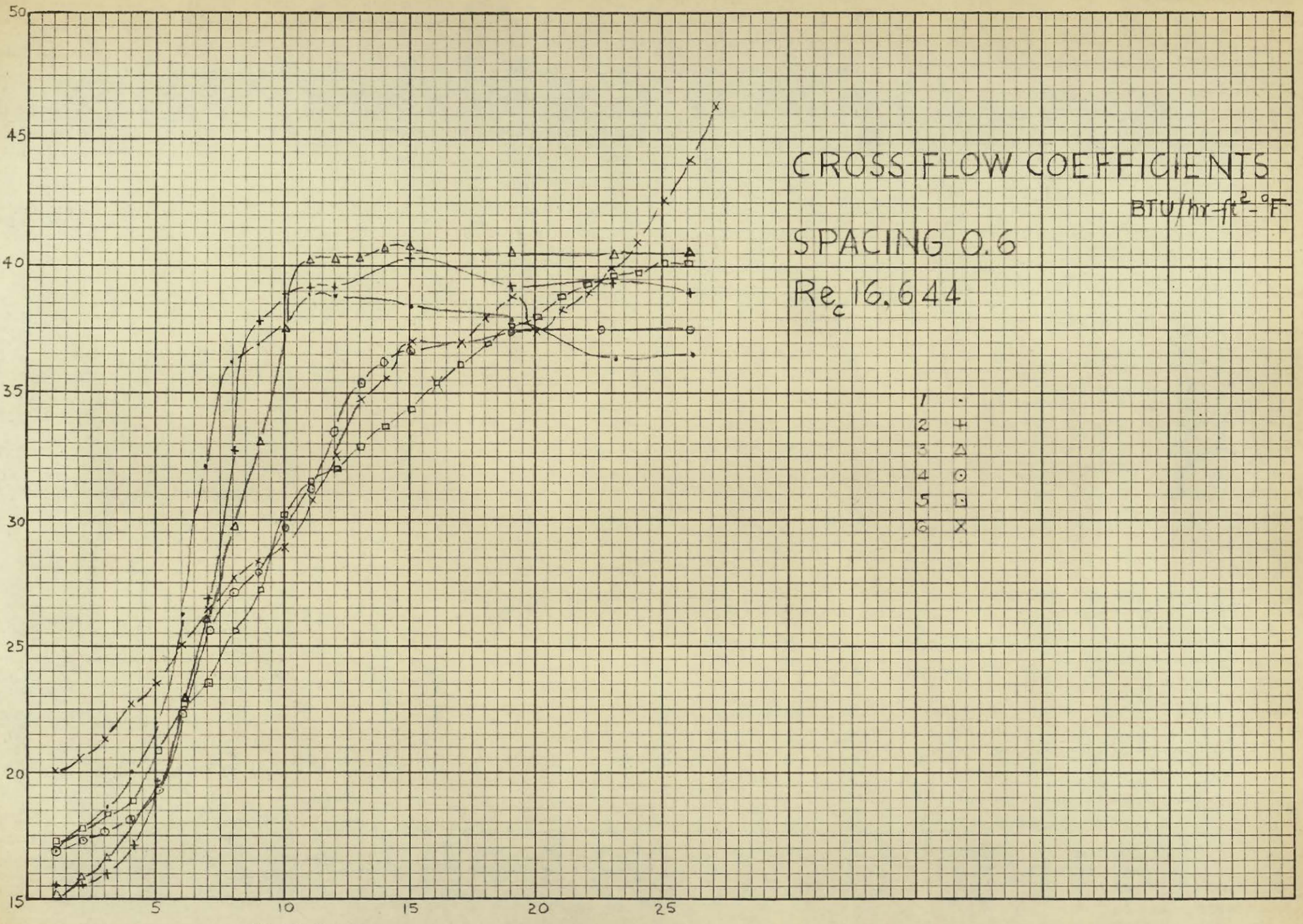

FIGURE 26.

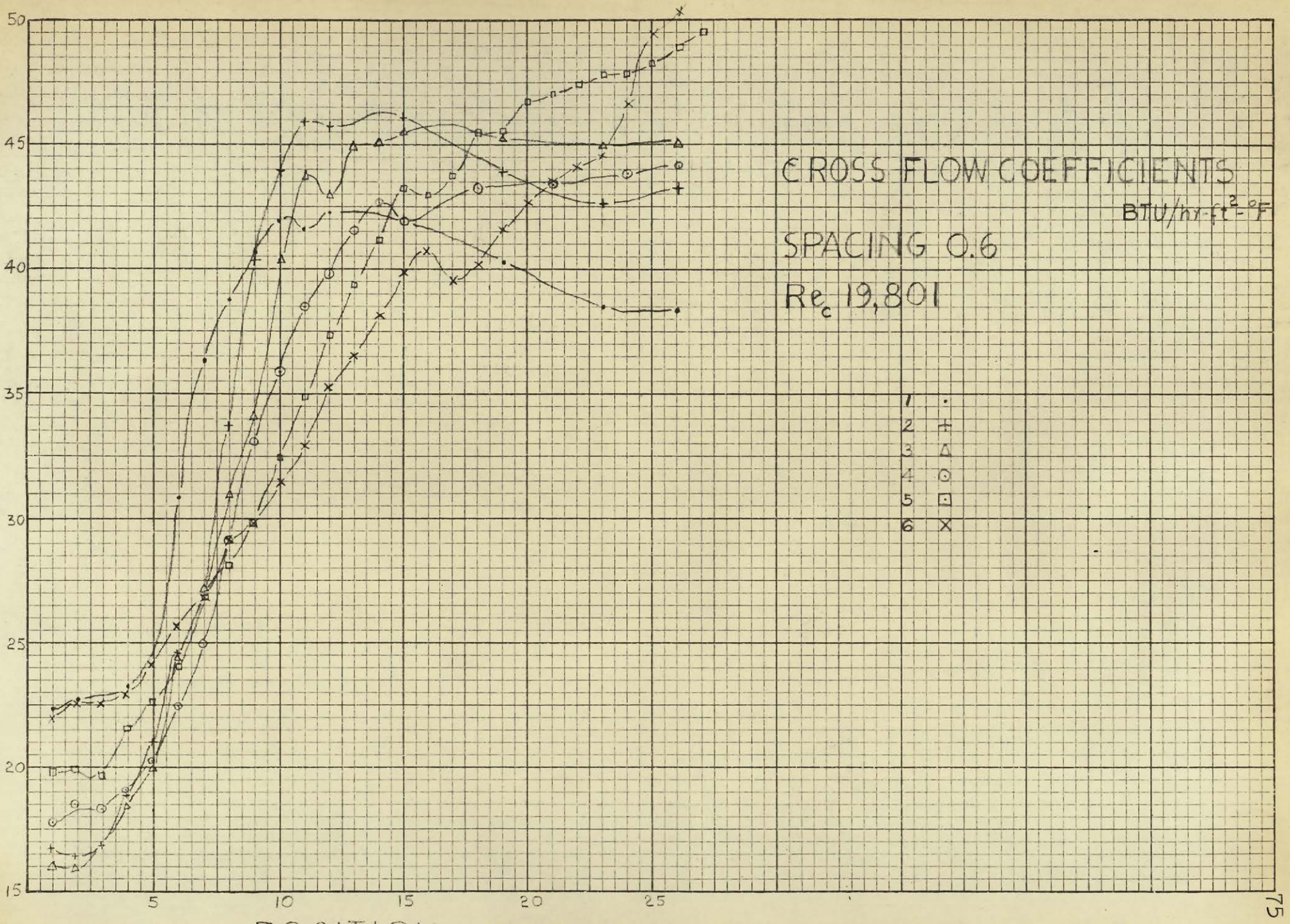

FIGURE 27.

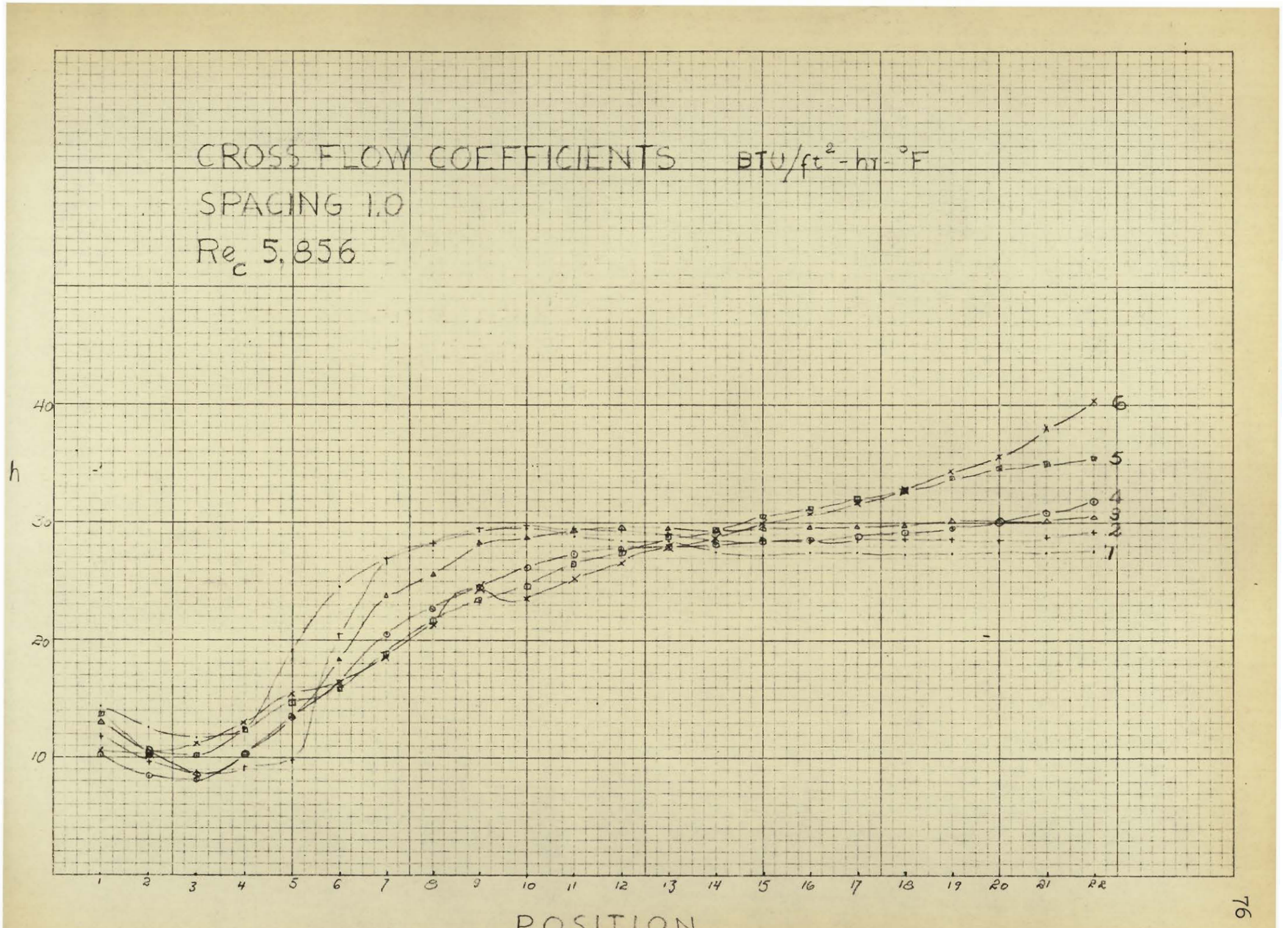

FIGURE 28.

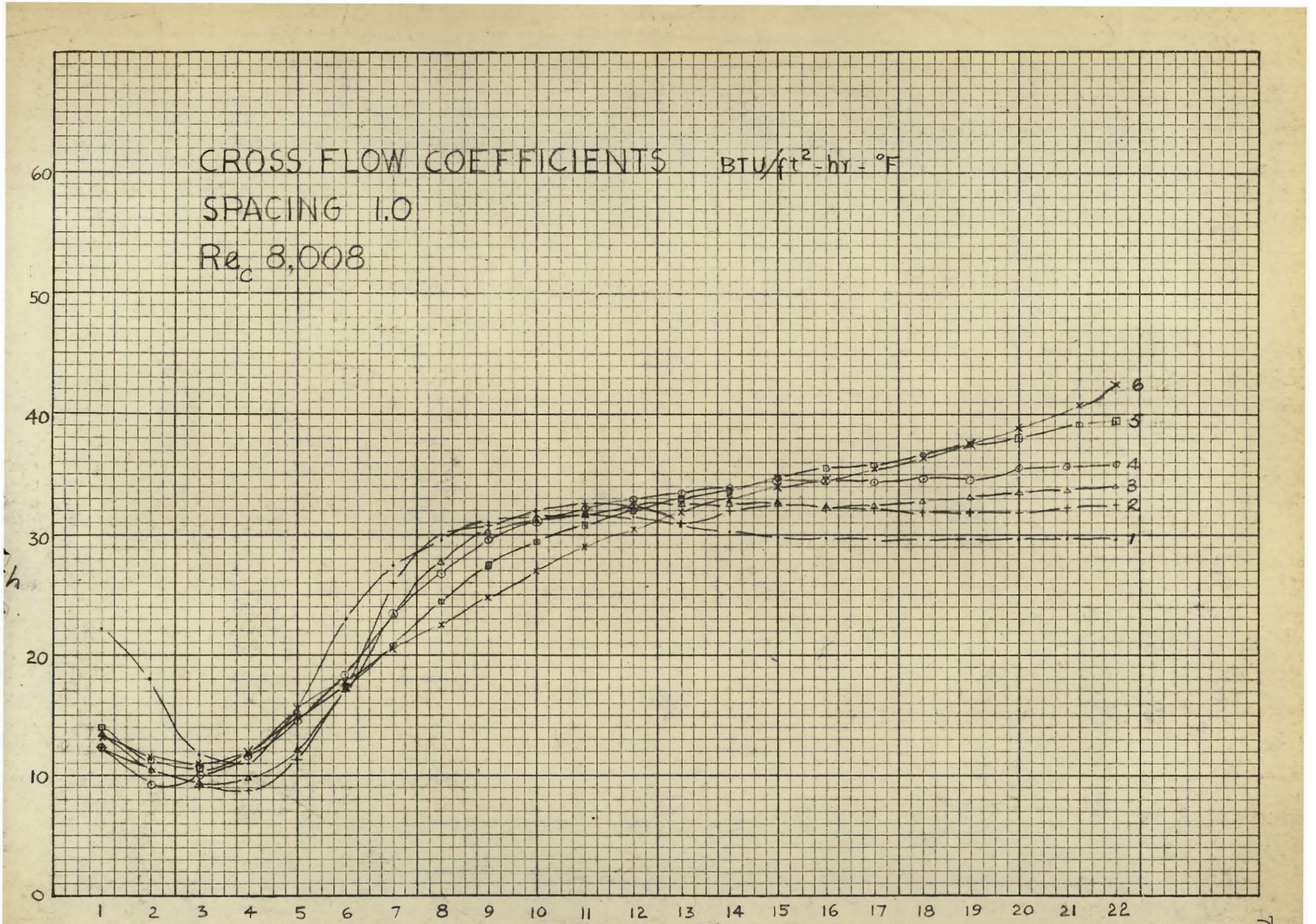

FIGURE 29.

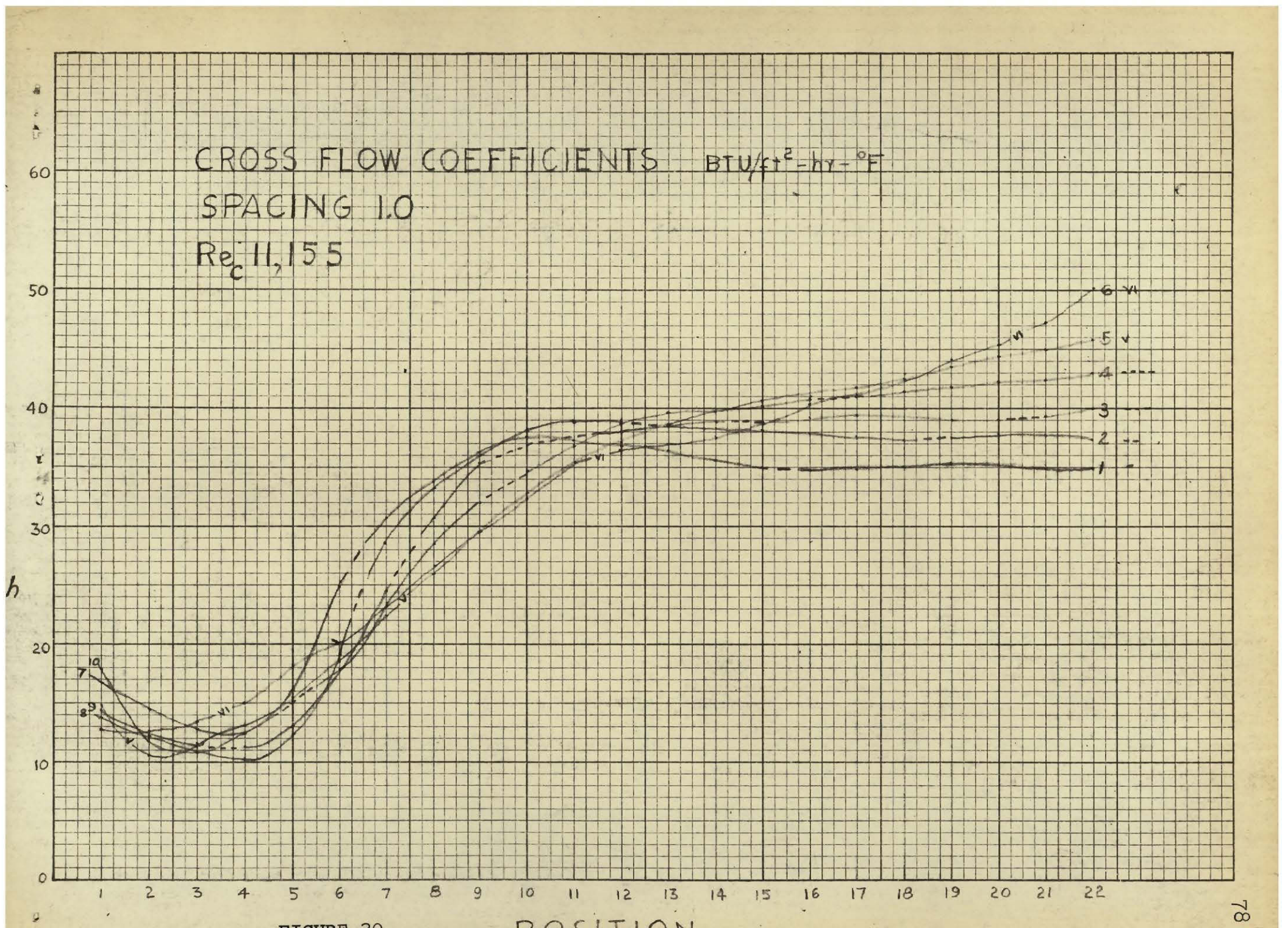

FIGURE 30.

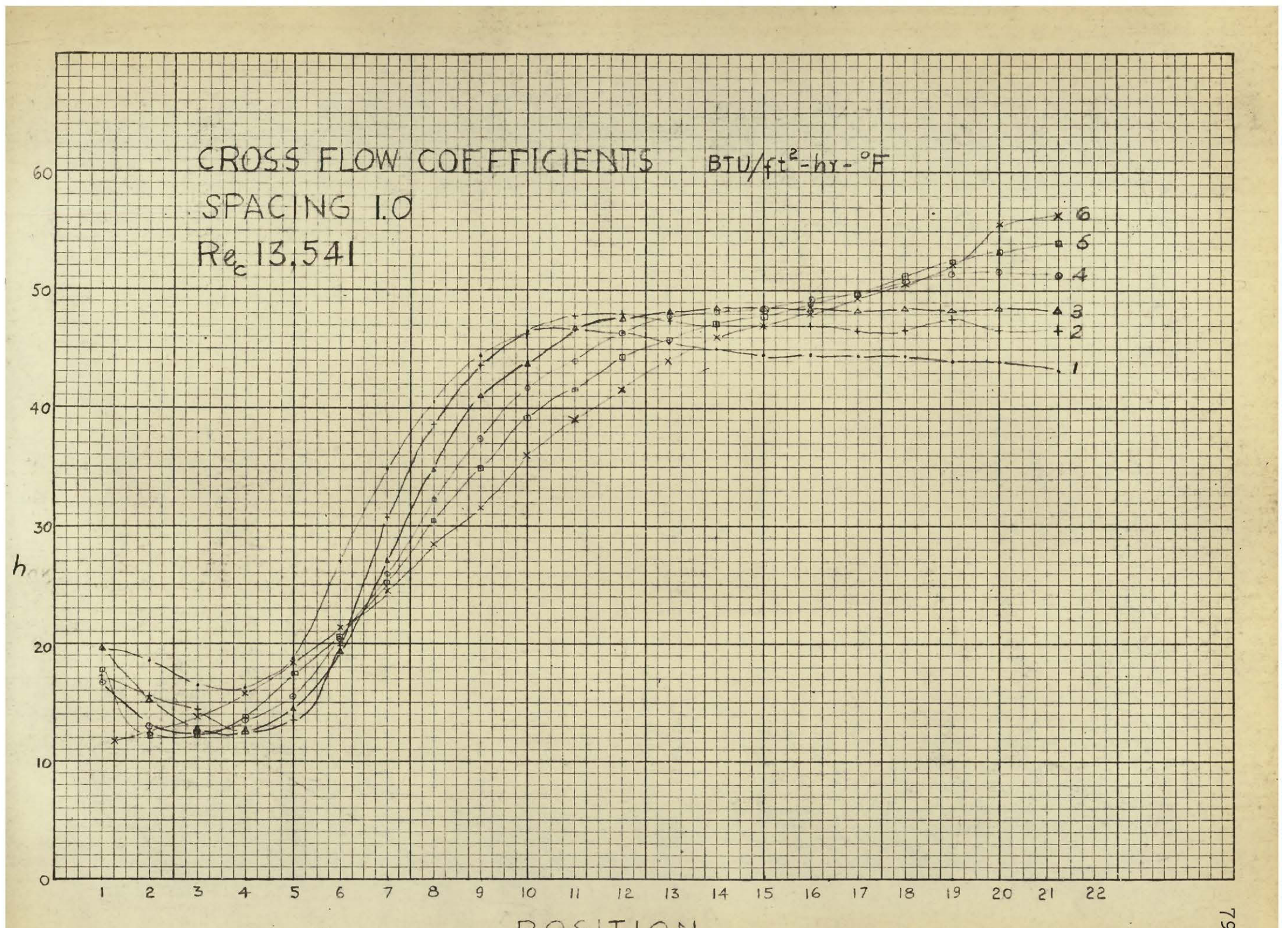

FIGURE 31.

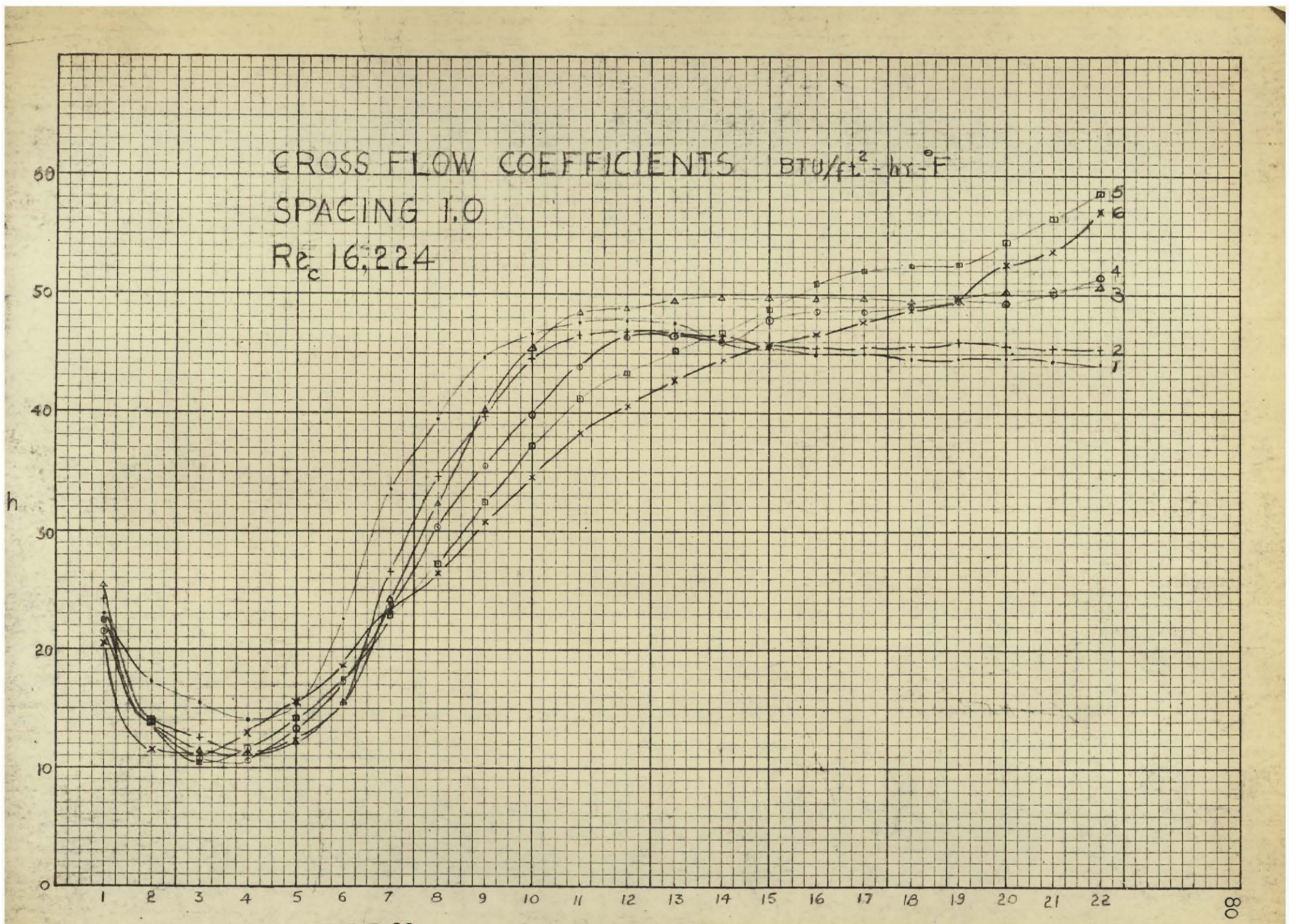

FIGURE 32.

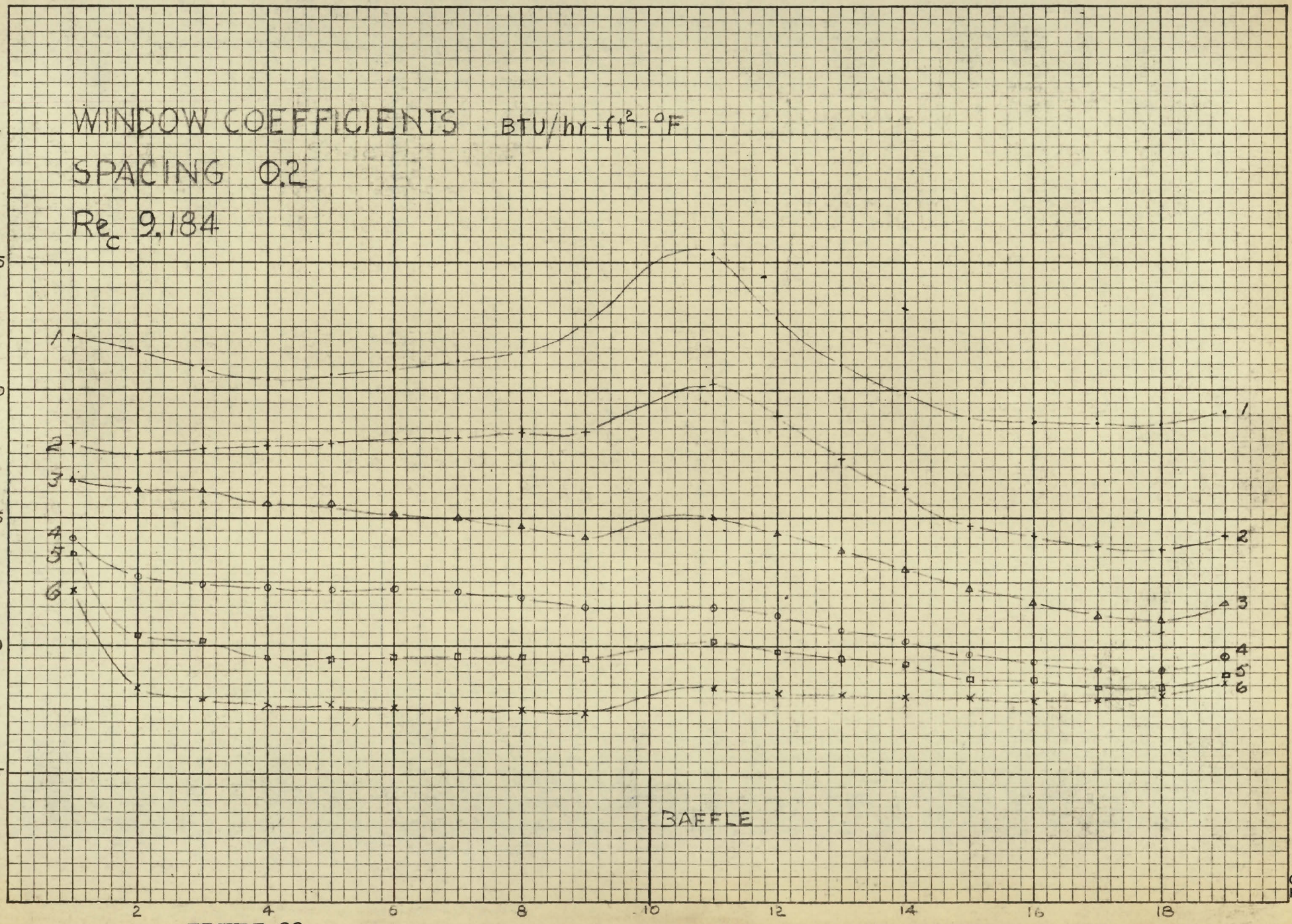

FIGURE 33.

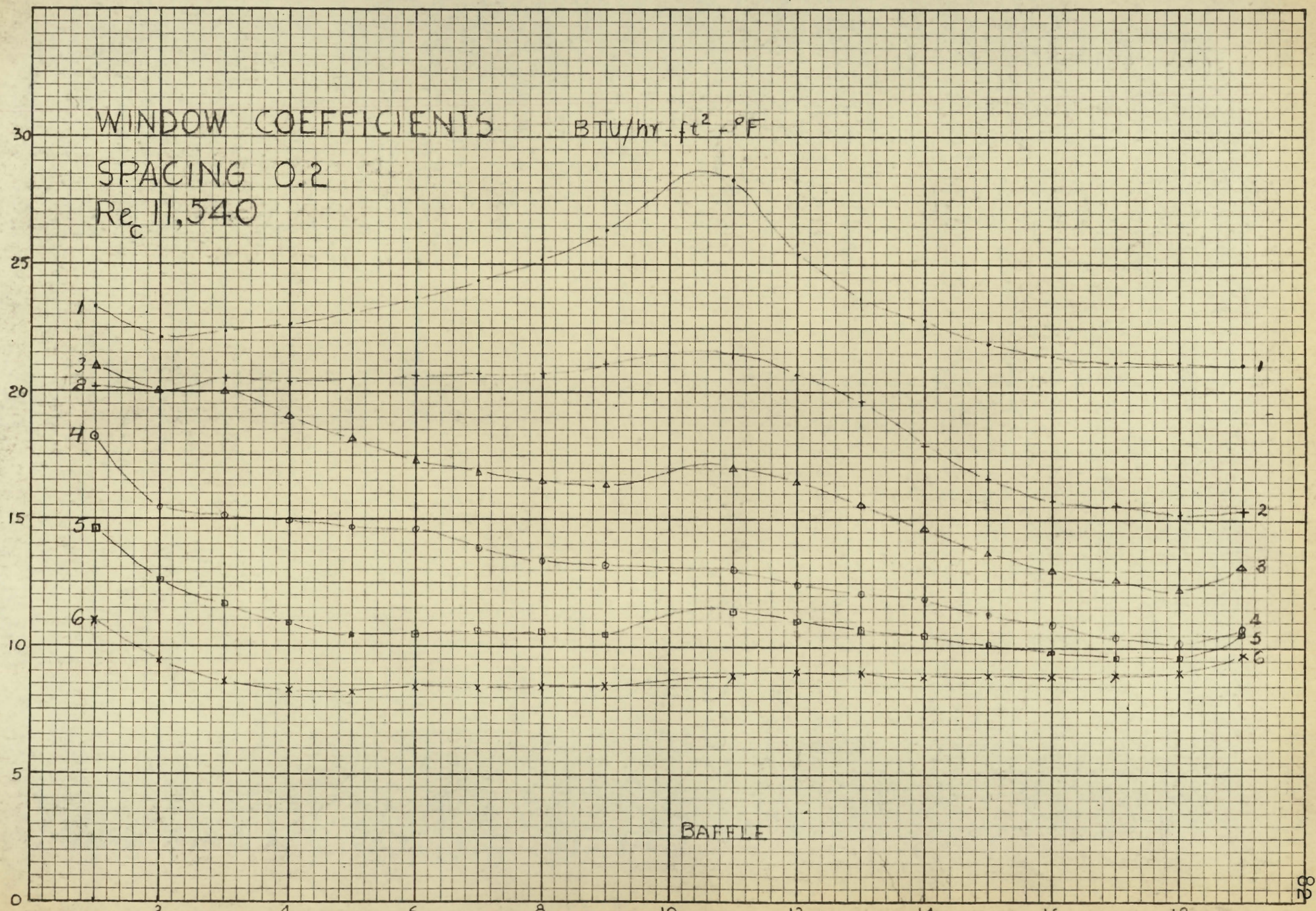

FIGURE 34.

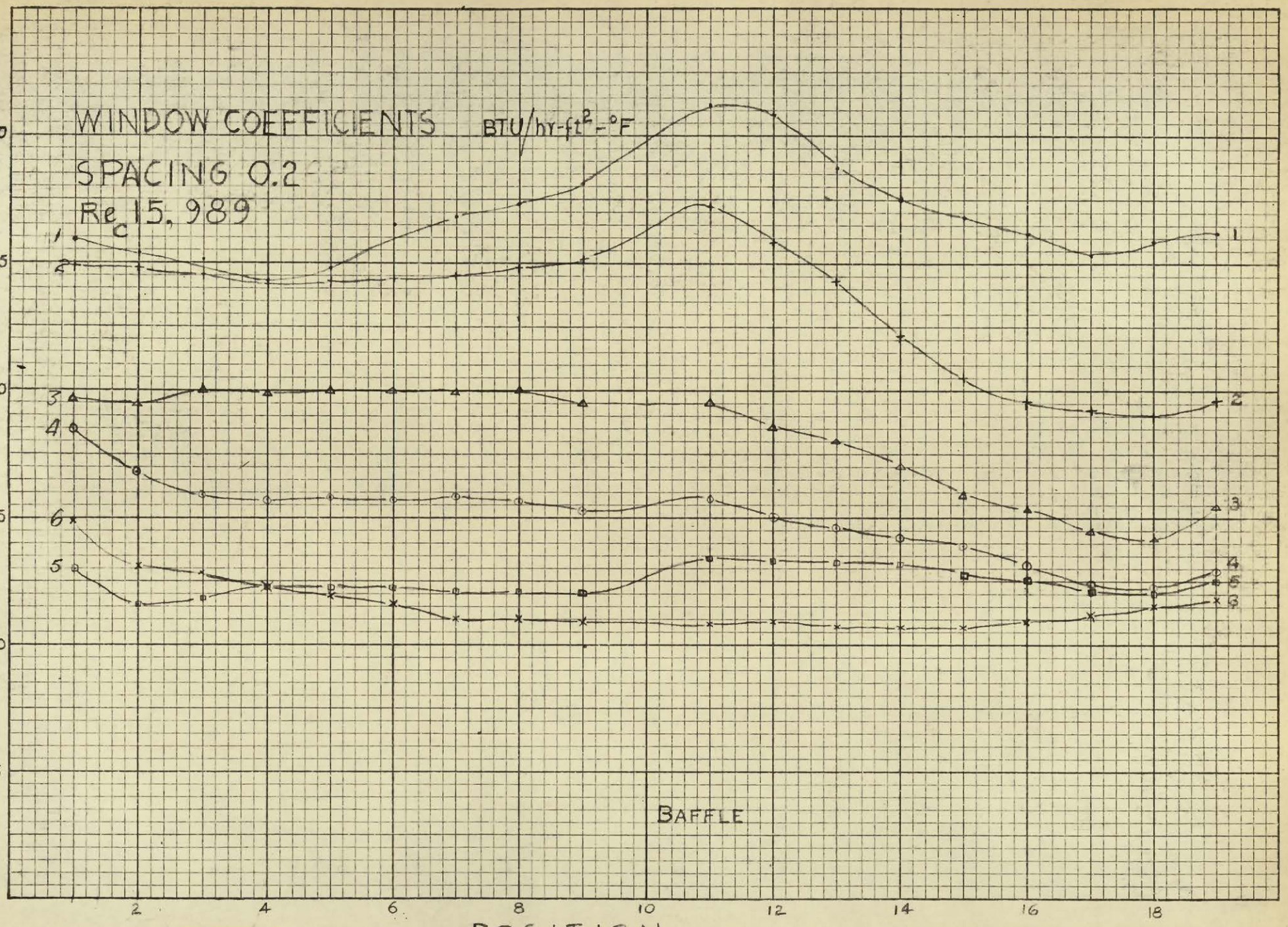

FIGURE 35.

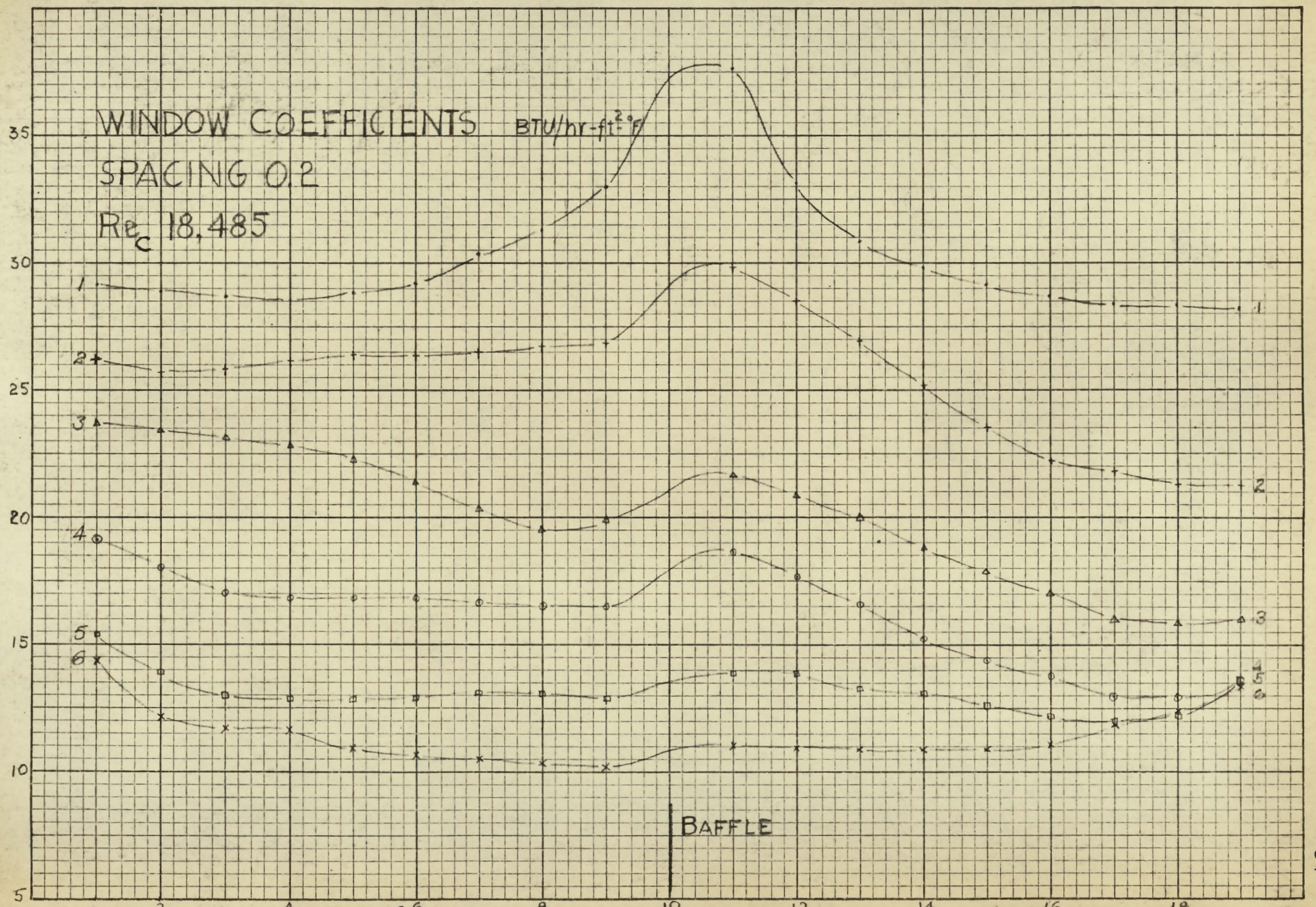

FIGURE 36.

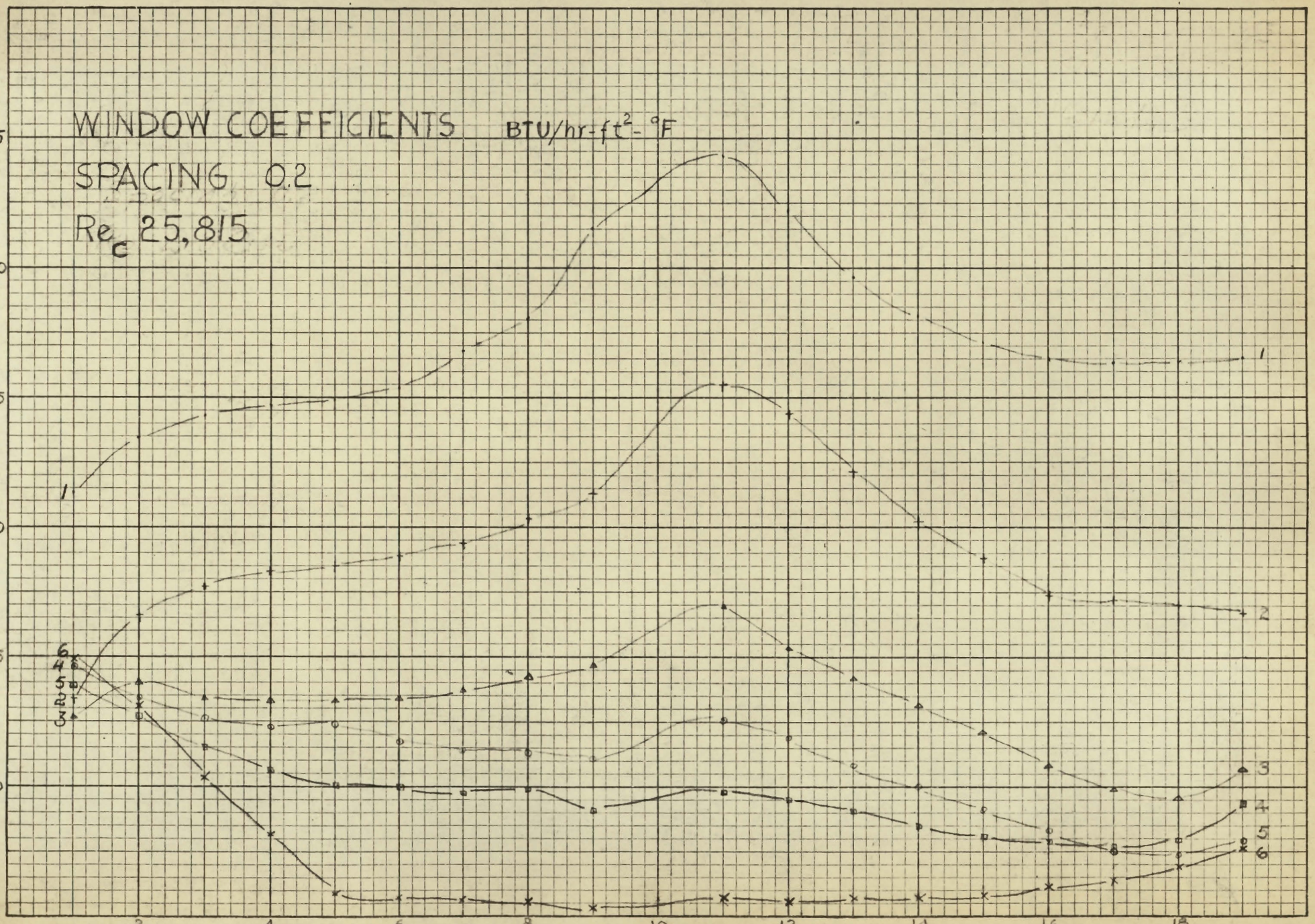

FIGURE 37.

WINDOW COEFFICIENTS BTU/hr-ft²-°F

SPACING 0.6

Re_c 5,552

1 •
2 +
3 △
4 ⊙
5 □
6 ×

h

60 56 52 48 44 40 36 32 28 24 20 16 12 8 4

2 4 6 8 10 12 14 16 18 20 22 24 26 28 30 32 34 36 38 40 42 44 46 48 50 52 54 56

BAFFLE

POSITION

FIGURE 38.

4.

WINDOW COEFFICIENTS BTU/hr-ft²-°F

SPACING 0.6

Re_c 7,790

1 ·
2 +
3 △
4 ⊙
5 ⊡
6 X

h

60 56 52 48 44 40 36 32 28 24 20 16 12 8 4

2 4 6 8 10 12 14 16 18 20 22 24 26 28 30 32 34 36 38 40 42 44 46 48 50 52 54 56

BAFFLE

POSITION

1 2 3 4 5 6

FIGURE 39.

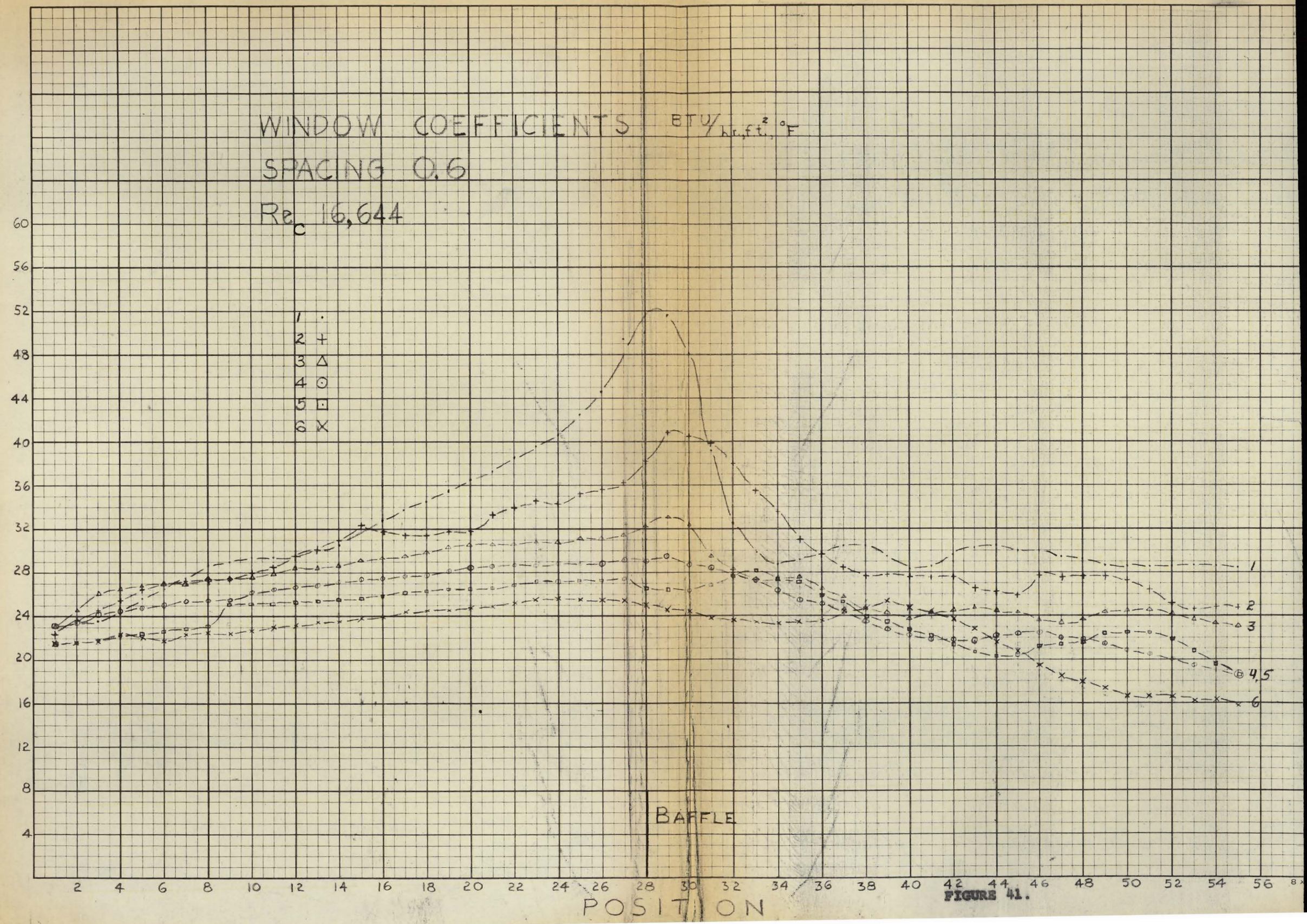
WINDOW COEFFICIENTS BTU/hr.ft.² °F
SPACING 0.6
Re_c 16,644
1 ·
2 +
3 △
4 ○
5 □
6 X
h av.
60
56
52
48
44
40
36
32
28
24
20
16
12
8
4
2 4 6 8 10 12 14 16 18 20 22 24 26 28 30 32 34 36 38 40 42 44 46 48 50 52 54 56
BAFFLE
POSITION
1
2
3
4,5
6

FIGURE 41.

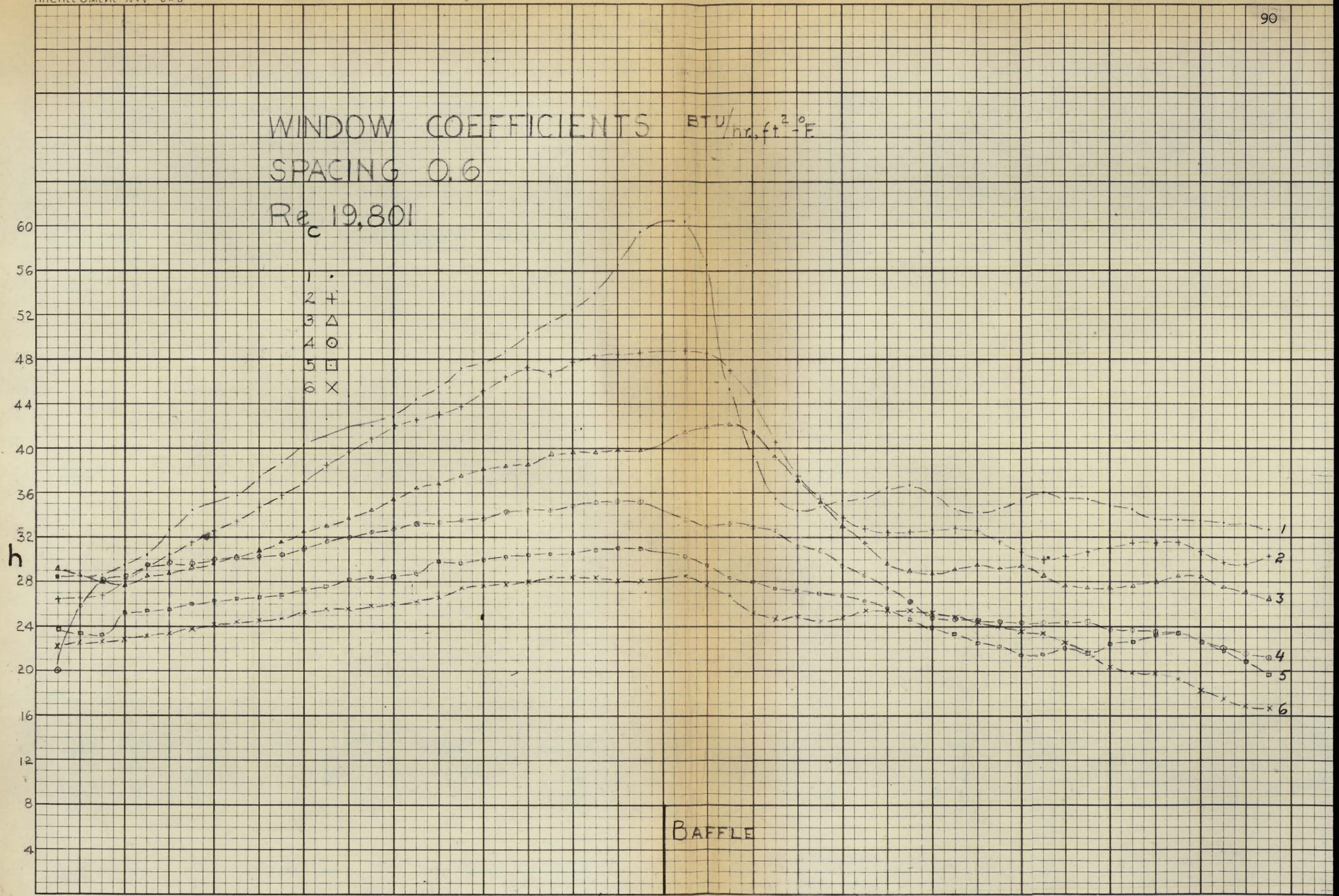
WINDOW COEFFICIENTS BTU/hr.ft²-°F
SPACING 0.6
Re_c 19,801
1 ·
2 +
3 △
4 ⊙
5 ⊡
6 ×
h
60
56
52
48
44
40
36
32
28
24
20
16
12
8
4
2 4 6 8 10 12 14 16 18 20 22 24 26 28 30 32 34 36 38 40 42 44 46 48 50 52 54 56
BAFFLE
POSITION
1
2
3
4
5
6

FIGURE 42.

WINDOW COEFFICIENT BTU/Ft.^{2}-°F-hr

SPACING 1.0

Re_c 5,856

1 •
2 +
3 △
4 ⊙
5 □
6 ×

h

52
48
44
40
36
32
28
24
20
16
12
8
4

13
14
15
16
17
18

1
2
3
4
5
6

BAFFLE

HUGHES OWENS 314A - 8 x 8

2 4 6 8 10 12 14 16 18 20 22 24 26 28 30 32 34 36 38 40 42 44 46 48 50 52 54 56

POSITION

FIGURE 43.

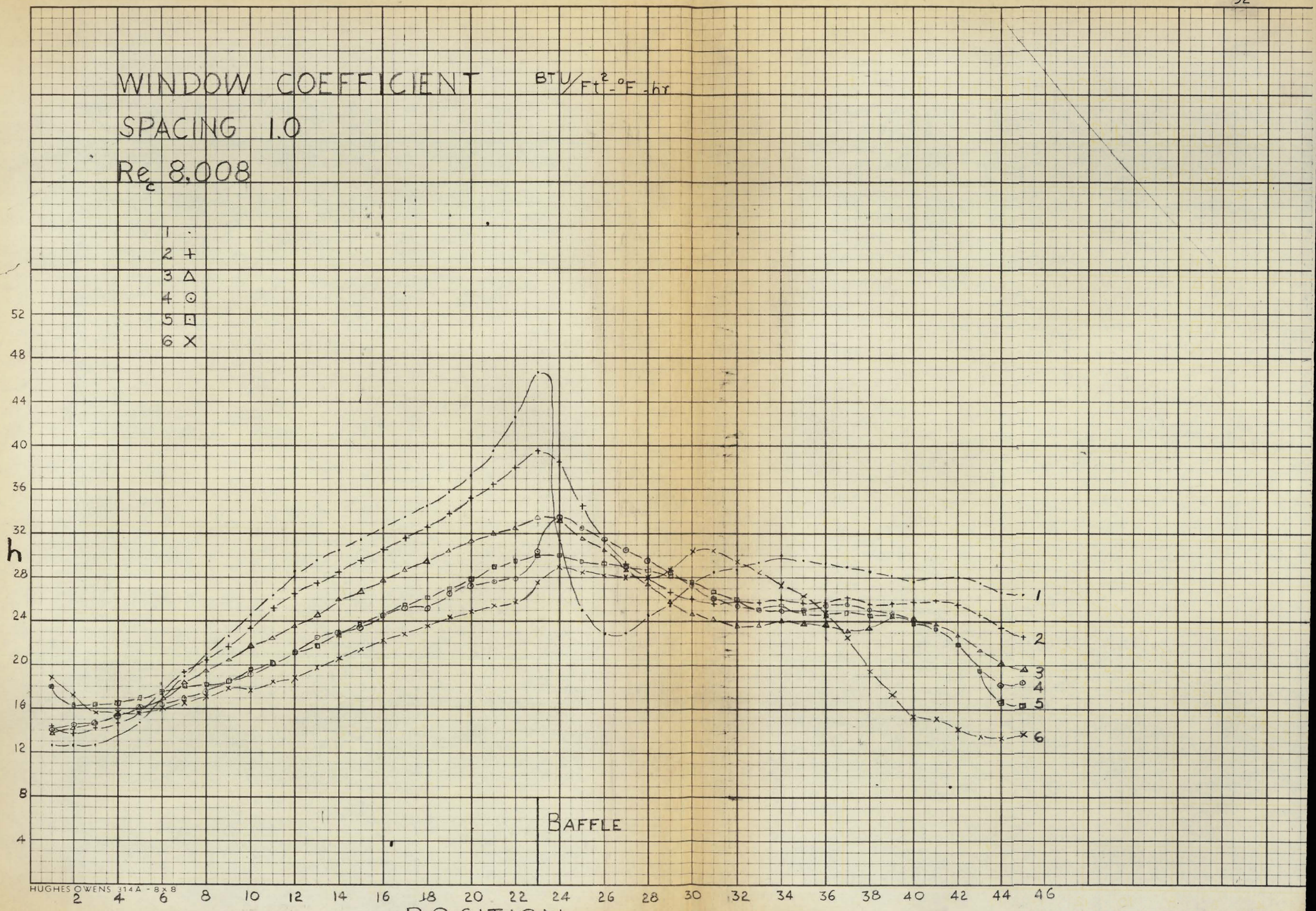
WINDOW COEFFICIENT BTU/Ft²-°F-hr
SPACING 1.0
Re_c 8.008
1 ·
2 +
3 △
4 ⊙
5 □
6 X
h
52
48
44
40
36
32
28
24
20
16
12
8
4
BAFFLE
2 4 6 8 10 12 14 16 18 20 22 24 26 28 30 32 34 36 38 40 42 44 46
POSITION
1
2
3
4
5
6
HUGHES OWENS 314A - 8X8

FIGURE 44.

WINDOW COEFFICIENT BTU/Ft²-°F-hr

SPACING 1.0

Re_c 11,155

1 ·
2 +
3 △
4 ⊙
5 ⊡
6 X

h

52
48
44
40
36
32
28
24
20
16
12
8
4

2 4 6 8 10 12 14 16 18 20 22 24 26 28 30 32 34 36 38 40 42 44 46 48 50

POSITION

BAFFLE

1
2
3
4
5
6

FIGURE 45.

WINDOW COEFFICIENT

SPACING 1.0

Re 13,541

h BTU/Ft² - °F - hr

1 ·
2 +
3 Δ
4 ⊙
5 ⊡
6 ×

64 60 56 52 48 44 40 36 32 28 24 20 16 12 8 4

2 4 6 8 10 12 14 16 18 20 22 24 26 28 30 32 34 36 38 40 42 44 46 48 50

POSITION

BAFFLE

FIGURE 46.

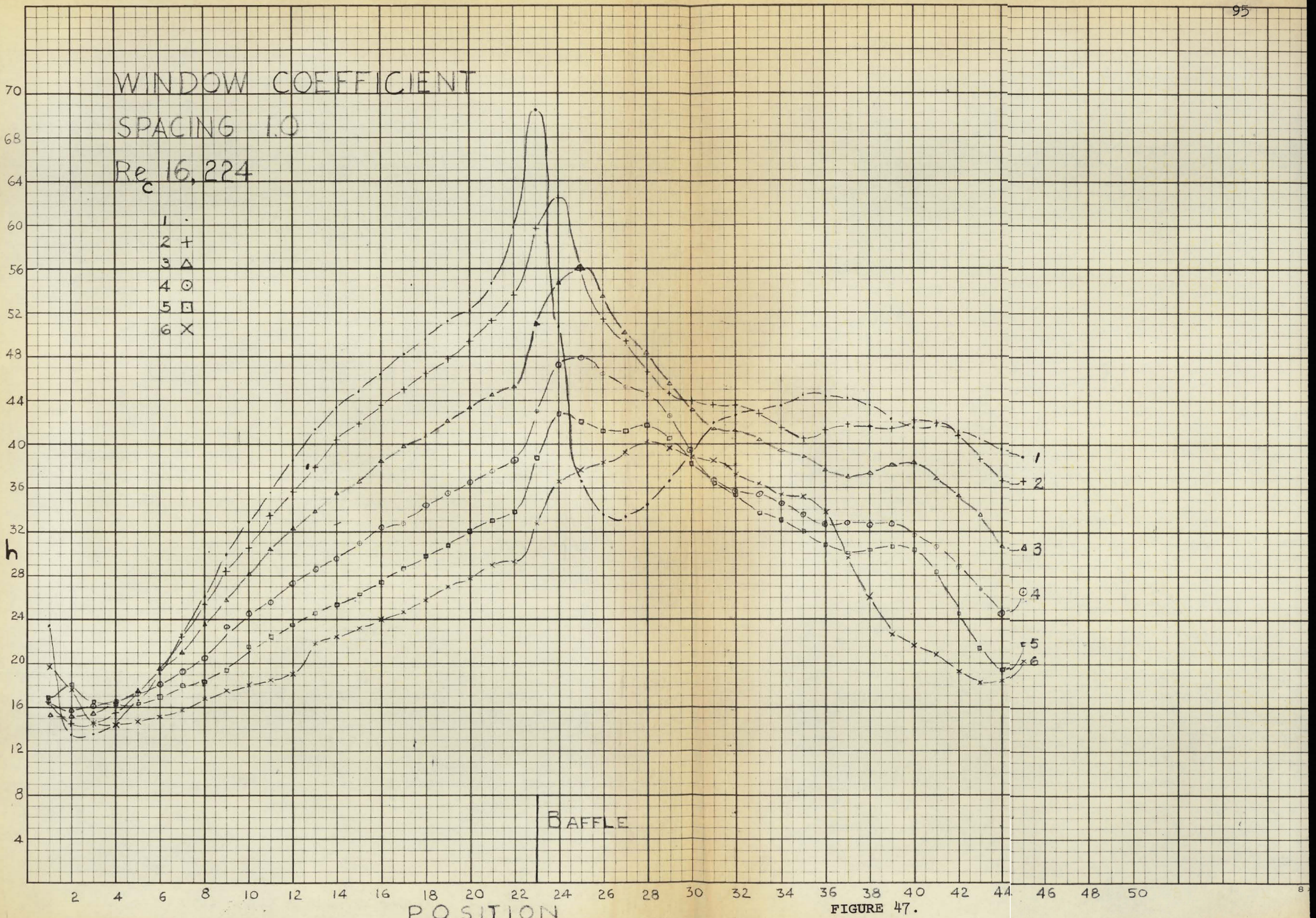
WINDOW COEFFICIENT
SPACING 1.0
Re_c 16,224
1 ·
2 +
3 △
4 ⊙
5 □
6 X
h
70
68
64
60
56
52
48
44
40
36
32
28
24
20
16
12
8
4
2 4 6 8 10 12 14 16 18 20 22 24 26 28 30 32 34 36 38 40 42 44 46 48 50
POSITION
BAFFLE
1
2
3
4
5
6

FIGURE 47.